Discrete Event Dynamic Systems (2020) 30:125–153
https://doi.org/10.1007/s10626-019-00298-6

Stochastic flow models with delays, blocking and applications to multi-intersection traffic light control

Rui Chen[1] · **Christos G. Cassandras**[1]

Received: 4 December 2018 / Accepted: 17 October 2019 /Published online: 30 December 2019

Abstract
We extend Stochastic Flow Models (SFMs), used for a large class of discrete event and hybrid systems, by including the delays which typically arise in flow movements, as well as blocking effects due to space constraints. We apply this framework to the multi-intersection traffic light control problem by including transit delays for vehicles moving from one intersection to the next and possible blocking between two intersections. Using Infinitesimal Perturbation Analysis (IPA) for this SFM with delays and possible blocking, we derive new on-line gradient estimates of several congestion cost metrics with respect to the controllable green and red cycle lengths. The IPA estimators are used to iteratively adjust light cycle lengths to improve performance and, in conjunction with a standard gradient-based algorithm, to obtain optimal values which adapt to changing traffic conditions. We introduce two new cost metrics to better capture congestions and show that the inclusion of delays and possible blocking in our analysis lead to improved performance relative to models that ignore delays and/or blocking effects.

Keywords Performance evaluation · Optimization · Discrete approaches for hybrid systems · Applications

1 Introduction

Stochastic Flow Models (SFMs) capture the dynamic behavior of a large class of hybrid systems (see Cassandras and Lafortune 2009). In addition, they are used as abstractions of Discrete Event Systems (DES), for example when discrete entities accessing resources

This article belongs to the Topical Collection: *Applications-2020*
Guest Editors: Francesco Basile, Jan Komenda, and Christoforos Hadjicostis

✉ Rui Chen
ruic@bu.edu

Christos G. Cassandras
cgc@bu.edu

[1] Division of Systems Engineering, Boston University, Brookline, MA, USA

are treated as flows. The basic building block in a SFM is a queue (buffer) whose fluid content is dependent on incoming and outgoing flows which may be controllable. By connecting such building blocks together, stochastic flow networks can be generated which are encountered in application areas such as manufacturing systems (Armony et al. 2015), water resources (Anderson et al. 2015), chemical processes (Yin et al. 2013), communication networks (Cassandras et al. 2002) and transportation systems (Geng and Cassandras 2015). Figure 1 shows a two-node SFM, in which an on-off switch controls the outgoing flow for each node. When the switch at the output of node 1 is turned on, a "flow burst" is generated to join the downstream node 2. Flow models commonly assume that this flow burst can instantaneously join the downstream queue, thus ignoring potentially significant delays before this can occur. Incorporating such delays through more accurate modeling is challenging but crucial in better evaluating the performance of the underlying system and seeking ways to improve it.

Control mechanisms used in SFMs often involve gradient-based methods in which the controller uses estimates of the performance metric sensitivities with respect to controllable parameters so as to adjust the values of these parameters and improve (ideally, optimize) performance. Infinitesimal Perturbation Analysis (IPA) is a method of general applicability to stochastic hybrid systems (see Cassandras et al. 2010; Wardi et al. 2010) through which gradients of performance measures can be estimated with respect to several controllable parameters based on directly observable data. The applications of IPA and its advantages have been reported elsewhere (e.g., Cassandras et al. 2010; Fleck et al. 2016) and are summarized here as follows: (i) IPA estimates are shown to be unbiased under very mild conditions (Cassandras et al. 2010). (ii) IPA estimators are robust with respect to the stochastic processes involved. (iii) IPA is event-driven, hence scalable in the number of events in the system, not the (much larger) state space dimensionality. (iv) IPA possesses a decomposability property (Yao and Cassandras 2011), i.e., IPA state derivatives become memoryless after certain events occur. (v) The IPA methodology can be easily implemented on line, allowing us to take advantage of directly observable data.

While IPA has been extensively used in SFMs, the effect of delays between adjacent nodes, as described above, has not been studied to date. Therefore, the first contribution of this paper is to incorporate delays in the flow bursts that are created by on-off switching control (see Fig. 1) into the standard SFM and to develop necessary extensions to IPA for such systems. Extending the original model introduced in Chen and Cassandras (2018), we include the possibility of multiple flow bursts arising between two nodes. While in Chen and Cassandras (2018) the capacity between two nodes was assumed to be infinite, the second contribution of this paper is to allow for a finite capacity and analyze the effect of possible blocking that may arise. The third contribution is to include an application of SFMs with delays and blocking to the Traffic Light Control (TLC) problem in transportation networks.

The rest of the paper is organized as follows. In Section 2, we extend the standard multi-node SFM to include delays. In Section 3 we adapt this model to the TLC problem by explicitly modeling the delay experienced by vehicles moving from one intersection to the next. This allows us to introduce two new cost metrics for congestion that incorporate the effect of delays. In Section 4, we carry out IPA for the TLC problem with delays and in Section 5 we extend our analysis to include blocking effects. In Section 6, we provide simulation examples comparing performance results first between a model considering traffic delays and one which does not, showing that the former achieves improved performance. We then include blocking effects and show how their inclusion in optimizing traffic light settings further improves performance.

2 Stochastic flow models with delays

Consider a two-node SFM as in Fig. 1 and let $\{\alpha_i(t)\}$ and $\{\beta_i(t)\}$, $i = 1, 2$, be the *incoming flow* and *outgoing flow processes* respectively. We emphasize that these are both treated as stochastic processes. We define $x(t) = [x_1(t), x_2(t)]$, where $x_i(t) \in \mathbb{R}^+$ is the flow content of node i (we assume that all variables are left-continuous). The dynamics of this SFM are

$$\dot{x}_i(t) = \begin{cases} 0 & \text{if } x_i(t) = 0,\ \alpha_i(t) \le \beta_i(t) \\ & \text{or } x_i(t) = c_i,\ \alpha_i(t) \ge \beta_i(t) \\ \alpha_i(t) - \beta_i(t) & \text{otherwise} \end{cases} \tag{1}$$

where c_i is the content capacity of i. The physical meaning of $x_i(t)$ depends on the application context. For example, in water resources (Anderson et al. 2015), $x_i(t)$ may be the water volume of a tank i, $\alpha_i(t)$ the incoming water rate to tank i and $\beta_i(t)$ the outgoing water rate from tank i. In the TLC problem, $x_i(t)$ is defined as the queue length of road i, $\alpha_i(t)$ is the incoming traffic flow rate and $\beta_i(t)$ is the outgoing traffic flow rate from road i.

$\beta_i(t)$ is defined as

$$\beta_i(t) = \begin{cases} h_i(t) & \text{if } G_i(t) = 1 \\ 0 & \text{otherwise} \end{cases} \tag{2}$$

in which $h_i(t)$ is the instantaneous outgoing flow rate at node i, and $G_i(t) \in \{0, 1\}$, $i = 1, 2$ is a switching controller. We also define a clock state variable $z_i(t)$ for each switching controller $G_i(t)$:

$$\begin{aligned} \dot{z}_i(t) &= \begin{cases} 1 & \text{if } G_i(t) = 1 \\ 0 & \text{otherwise} \end{cases} \\ z_i(t^+) &= 0 \quad \text{if } G_i(t) = 1 \text{ and } G_i(t^+) = 0 \end{aligned} \tag{3}$$

Here we define $z_i(t^+)$ to be the value of $z_i(t)$ just after a discontinuity occurs at time t. This notation applies to all variables in the rest of the paper which may experience discontinuities when certain events take place. Thus, when $G_1(t) = 1$, $t \in [t_1, t_2)$, $G_1(t_1^-) = 0$, a flow burst is created at node 1 (when $x_1(t_1) > 0$). In general, several such flow bursts may be created over $(t_1, t_2]$, depending on the values of $\alpha_1(t)$, $h_1(t)$, $t \in (t_1, t_2]$. In SFMs studied to date, the delay incurred by any such flow burst being transferred between nodes has been ignored, assuming instead that it instantaneously joins the queue at node 2. Under this assumption,

$$\alpha_2(t) = \begin{cases} \alpha_1(t) & \text{if } x_1(t) = 0,\ \alpha_1(t) \le \beta_1(t) \\ \beta_1(t) & \text{otherwise} \end{cases}$$

In what follows, we extend the SFM to include the aforementioned delay which depends on when a flow burst actually joins the downstream queue, an event that we need to carefully specify. While a flow burst is in transit between nodes 1 and 2, let $x_{12}(t)$ be its size, i.e., the flow volume in transit before it joins $x_2(t)$. For simplicity, we assume that each flow

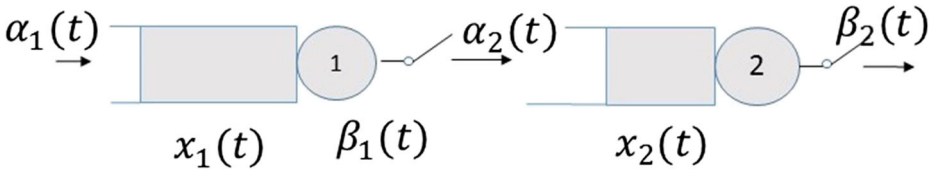

Fig. 1 A two-node SFM

burst is maintained during this process (i.e., the burst may not be separated into two or more sub-bursts). We will use L to denote the physical distance between nodes 1 and 2.

Predicting the time when the first flow burst actually joins queue 2 is complicated by the fact that $x_2(t)$ evolves while this burst is in transit. This is illustrated through the example in Fig. 2 which we will use to describe the evaluation of this time through a sequence of events denoted by $\{J_1, \ldots, J_K\}$ with associated event times $\{\sigma_1, \ldots, \sigma_K\}$. We define J_0 to be the event when the flow burst leaves node 1, i.e., the occurrence of a switch from $G_1(t^-) = 0$ to $G_i(t) = 1$, and let σ_0 be its associated occurrence time.

Therefore, an estimate of the time when the flow burst joins the tail of queue 2 is given by

$$\sigma_1 = \sigma_0 + [L - x_2(\sigma_0)]/v(\sigma_0)$$

where $v(\sigma_0)$ is the "speed" of the flow burst which we assume to be constant and, for notational simplicity, set it to $v(\sigma_0) = 1$ (it will become clear in the sequel that this can be relaxed and treated as random in the context of IPA). Thus, we define J_1 to be the event at time σ_1 when the flow burst covers the distance $L - x_2(\sigma_0)$. In general, however, $x_2(\sigma_1) \leq x_2(\sigma_0) \equiv \bar{x}_2(\sigma_1)$, i.e., the *estimate* $\bar{x}_2(\sigma_1)$ of $x_2(\sigma_1)$ is based on the assumption that $x_2(t)$ remains unchanged over (σ_0, σ_1). This is illustrated in the example of Fig. 2, where $\dot{x}_2(t) = -\beta_2(t) < 0$ for some $t \in (\sigma_0, \sigma_1)$. Therefore, unless $x_2(\sigma_1) = x_2(\sigma_0)$, we repeat at $t = \sigma_1$ the same process of estimating the time of the next opportunity that the flow burst might join queue 2 at time σ_2 to cover the distance $\bar{x}_2(\sigma_1) - x_2(\sigma_1)$ and define this potential *joining event* as J_2. This process continues until event J_K occurs at time σ_K, the last event in the sequence $\{J_1, \ldots, J_K\}$ when $\bar{x}_2(\sigma_K) = x_2(\sigma_K)$.

Note that J_K may occur either when (i) $\bar{x}_2(\sigma_K) = x_2(\sigma_K) > 0$, in which case the estimate $\bar{x}_2(\sigma_K)$ incurs no error because $x_2(\sigma_K) = x_2(\sigma_{K-1})$, i.e., the queue length at node 2 remained unchanged because $\beta_2(t) = 0$ for $t \in [\sigma_{K-1}, \sigma_K]$, or (ii) $\bar{x}_2(\sigma_K) = x_2(\sigma_K) = 0$, in which case the flow burst joins node 2 while this queue is empty. Since in practice the queues and flow bursts may consist of discrete entities (e.g., vehicles), we define event J_K

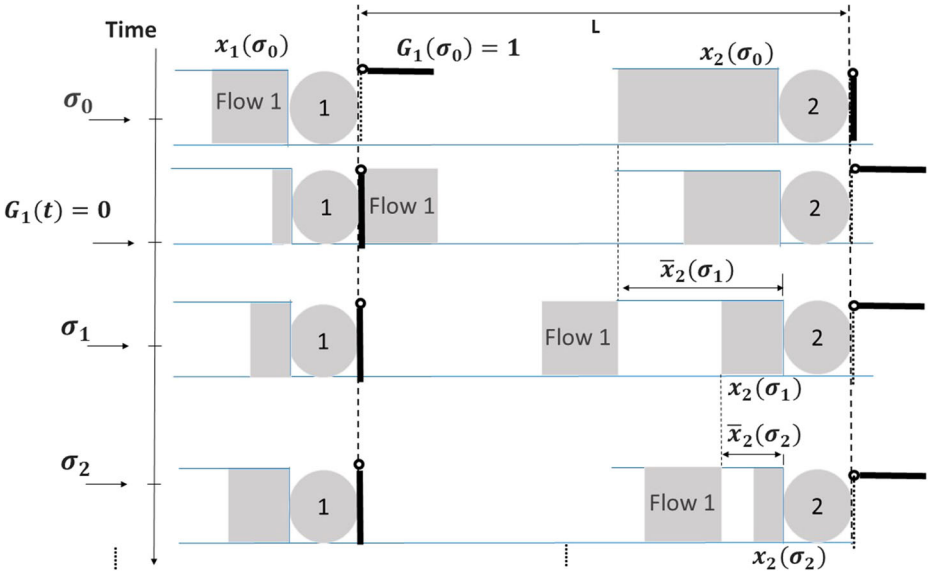

Fig. 2 Typical evolution of a flow burst in transit

as occurring when $\bar{x}_2(t) - x_2(t) \leq \epsilon$ for some predefined fixed small ϵ, i.e., a flow burst joins the downstream queue whenever it is sufficiently close to it. The following lemma asserts that the event time sequence $\{\sigma_1, \ldots, \sigma_K\}$ is finite.

Lemma 1 *Under the assumption that J_K is defined through $\bar{x}_2(\sigma_K) - x_2(\sigma_K) \leq \epsilon$, the number of events K in $\{J_1, \ldots, J_K\}$ is bounded. Moreover, its event time σ_K is also bounded.*

Proof Observe that $x_2(t) \leq L$, since the content of queue 2 is limited by the physical distance L. In addition, $\bar{x}_2(t) - x_2(t) > \epsilon$ prior to event J_K. It follows that $K \leq L/\epsilon$. Moreover, in the worst case, a flow burst travels the finite distance L to find $x_2(\sigma_K) = 0$, therefore, $\sigma_K \leq \sigma_0 + L - x_2(\sigma_0)$. □

We now formalize the dynamics of the flow transit process described above. First, the dynamics of $\bar{x}_2(t)$, the estimated queue length when an event J_k occurs, are given by

$$\begin{aligned} \dot{\bar{x}}_2(t) &= 0 \\ \bar{x}_2(t^+) &= x_2(t) \text{ if } t = \sigma_k, k = 1, ..., K. \end{aligned} \tag{4}$$

with $\bar{x}_2(\sigma_1) = L - x_2(\sigma_0)$ and σ_0 defined above as the occurrence time of a switch from $G_1(t^-) = 0$ to $G_i(t) = 1$. The dynamics of $x_{12}(t)$ are given by

$$\begin{aligned} \dot{x}_{12}(t) &= \begin{cases} 0 & \text{if } G_1(t) = 0 \\ \alpha_1(t) & \text{if } x_1(t) = 0,\ \alpha_1(t) \leq \beta_1(t) \\ h_1(t) & \text{otherwise} \end{cases} \\ x_{12}(t^+) &= 0 \quad \text{if } t = \sigma_K \end{aligned} \tag{5}$$

The dynamics of $x_2(t)$ are no longer described by Eq. 1, since an increase in the queue content is only updated when a flow burst joins queue 2 at time σ_K. Instead, they are given by

$$\begin{aligned} \dot{x}_2(t) &= \begin{cases} -\beta_i(t) & \text{if } x_2(t) > 0 \text{ and } G_2(t) = 1 \\ 0 & \text{otherwise} \end{cases} \\ x_2(\sigma_K^+) &= x_2(\sigma_K) + x_{12}(\sigma_K) \end{aligned} \tag{6}$$

Note that in Eqs. 4 and 5 the values of event times $\{\sigma_1, \ldots, \sigma_K\}$ are still unspecified. In order to provide this specification, we define

$$\delta_{12}(t) = \bar{x}_2(t) - x_2(t)$$

to be the distance between the head of the flow burst and the tail of $x_2(t)$. Then, observe that

$$\sigma_k = \sigma_{k-1} + \tau(\delta_{12}(\sigma_{k-1}))$$

where $\tau(r)$ is the time to complete a distance $r \in (0, L]$ and $k = 1, ..., K-1$. Similar to the clock $z_i(t)$ in Eq. 3 that dictates the timing of the controlled switching process, we associate a clock $z_{12}(t)$ to the timing of events in $\{J_1, \ldots, J_K\}$ as follows:

$$\begin{aligned} \dot{z}_{12}(t) &= \begin{cases} 1 & \text{if } \delta_{12}(t) > 0 \\ 0 & \text{otherwise} \end{cases} \\ z_{12}(t^+) &= 0 \quad \text{if } z_{12}(t) = \tau(\delta_{12}(t)) \end{aligned} \tag{7}$$

with an initial condition $z_{12}(\sigma_0) = 0$ and

$$\begin{aligned} \dot{\delta}_{12}(t) &= 0 \\ \delta_{12}(t^+) &= \begin{cases} L - x_2(t) & \text{if } t = \sigma_0 \\ \bar{x}_2(t) - x_2(t) & \text{if } t = \sigma_k, k = 1, ..., K. \end{cases} \end{aligned} \tag{8}$$

Note that $\delta_{12}(t)$ is piecewise constant and updated only at the times when events $J_0, J_1, \ldots, J_K$ take place ending with $\delta_{12}(t^+) = 0$ when event J_K occurs, i.e., the flow burst joins queue 2. The values of $\tau(\delta_{12}(t))$ in Eq. 7 are given by the time required for the flow burst to travel a distance $\delta_{12}(t) = \bar{x}_2(t) - x_2(t)$ with speed $v(\sigma_0)$ which we assumed earlier to be constant and set to $v(\sigma_0) = 1$. Thus, $\tau(\delta_{12}(t)) = \delta_{12}(t)$. Finally, note that in this modeling framework, we assume that $x_2(t)$ is observable at event times $\sigma_0, \sigma_1, \ldots, \sigma_K$ when events $J_0, J_1, \ldots, J_K$ take place.

As a final step, we generalize the model in Chen and Cassandras (2018) to include multiple flow bursts that may be generated in an interval $(t_1, t_2]$ such that $G_1(t) = 1$ for $t \in [t_1, t_2)$, $G_1(t_1^-) = 0$. Thus, we denote by J_k^n the kth event for the nth flow burst to (potentially) join queue 2 and extend $\delta_{12}(t)$ to $\delta_{12}^n(t)$, σ_k to σ_k^n, and $x_{12}(t)$ to $x_{12}^n(t)$, $n = 1, 2, \ldots$ Also, we define $J_{i,j}$ as an event such that the ith flow burst merges with the jth burst at time $\tau_{i,j}$. For simplicity, we use $y^m(t)$ to represent $x_{12}^m(t)$. We then have:

$$\dot{x}_{12}^n(t) = \begin{cases} \alpha_1(t) & \text{if } n = 1, x_1(t) = 0,\ \alpha_1(t) < \beta_1(t) \\ h_1(t) & \text{if } n = 1, G_1(t) = 1 \\ & x_1(t) = 0,\ \alpha_1(t) \geq \beta_1(t) \text{ or } x_1(t) > 0 \\ 0 & \text{otherwise} \end{cases} \tag{9}$$

$$\begin{aligned} x_{12}^n(t^+) &= 0 \quad \text{if } t = \sigma_K^n \text{ or } t = \tau_{n,n-1} \\ x_{12}^n(t^+) &= x_{12}^n(t) + x_{12}^{n-1}(t) \quad \text{if } t = \tau_{n+1,n} \end{aligned} \tag{10}$$

$$\begin{aligned} \dot{\delta}_{12}^n(t) &= 0 \\ \delta_{12}^n(t^+) &= \begin{cases} L - x_2(t) & \text{if } t = \sigma_0^n \\ \bar{x}_2^n(t) - x_2(t) & \text{if } t = \sigma_k^n, k > 0 \\ \delta_{12}^n(t) - y^m(t) & \text{if } t = \sigma_K^m, m = 1, \ldots, n-1 \end{cases} \end{aligned} \tag{11}$$

$$\begin{aligned} \dot{\bar{x}}_2^n(t) &= 0 \\ \bar{x}_2^n(t^+) &= \begin{cases} x_2(t) & \text{if } t = \sigma_k^n, k \geq 0 \\ \bar{x}_2^n(t) + y^m(t) & \text{if } t = \sigma_K^m, m = 1, \ldots, n-1 \end{cases} \end{aligned} \tag{12}$$

with the obvious generalizations of Eqs. 4-8.

The generalized SFM with delays is shown in Fig. 3. We define a series of servers d_n, $n \in \{j \in \mathbb{Z} : j = 1, \ldots, N\}$ to describe the flow transit delay between SFM where $y_n(t)$ is the content of d_n. Here, N is the total number of servers required depending on a specific application. For example, in the two-intersection traffic system discussed in the next section, we set $N = \lceil L/L_v \rceil$ where L is the physical distance between intersections and L_v is the length of a vehicle. When a new flow burst leaves server 1, the controlled switching process checks whether $y_1(t) = 0$ to initiate a flow burst. If $y_1(t) > 0$, it checks $y_j(t)$ for $j \geq 2$ until $y_j(t) = 0$ for some j. For example, in Fig. 3, if servers d_1 and d_2 are non-empty (dark color), and d_3 is empty (light color), the new flow burst will join server d_3 until $y_1(t) = 0$. The first flow burst will leave server d_1 when event J_K^1 occurs and joins $x_2(t)$. The flow burst in server d_n will leave when either one of two events occurs, defined as follows: (1)

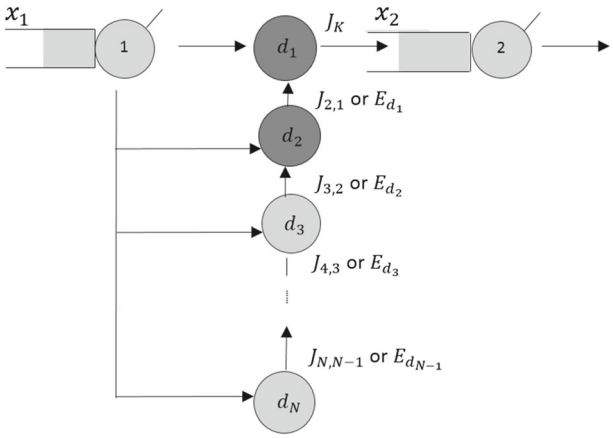

Fig. 3 Two-node SFM with delay

$J_{n,n-1}$ occurs when the nth flow burst joins the $(n-1)$th burst. (2) $E_{d_{n-1}}$ occurs when $y_{n-1}(t) = 0$.

SFM Events The hybrid system with dynamics given by Eqs. 1-8 defines the SFM with transit delays. To complete the model, we define next the event set associated with all discontinuous state transitions in Eqs. 1-8. As in prior work using SFMs, we observe that the sample path of any queue content process in our model can be partitioned into *Non-Empty Periods* (NEPs) when $x_i(t) > 0$, and *Empty Periods* (EPs) when $x_i(t) = 0$. Let us define the start of a NEP at queue i as event S_i (S_{12} for queue 12) and the end of a NEP at queue i as event E_i (E_{12} for queue 12). In Eq. 1, observe that S_1 is an event that can be induced by either an event such that $\alpha_1(t) - \beta_2(t)$ switches from ≤ 0 to > 0 or by an event which switches the value of $\beta_1(t)$; moreover, in Eq. 2, the value of $\beta_1(t)$ switches when an event occurs such that $G_1(t)$ changes between 0 and 1. In Eq. 6, S_2 may also be induced by event J_k if it occurs when $x_2(t) = 0$. Finally, in Eq. 5, S_{12} is induced by the same events that induce S_2, while E_{12} is induced by J_K since that causes the end of the flow burst that created $x_{12}(t) > 0$. To sum up, assuming for now that $c_i = \infty$ in Eq. 1, there are five events that can affect any of the processes $\{x_1(t)\}$, $\{x_2(t)\}$ and $\{x_{12}(t)\}$:

1. E_i: $x_i(t)$ switches from > 0 to $= 0$, thus ending a NEP at queue i.
2. Γ_i: $\alpha_i(t) - \beta_i(t)$ switches from ≤ 0 to > 0.
3. J_k: $z_{12}(t) = \tau(\delta_{12}(t))$ representing a potential joining of the flow burst $x_{12}(t)$ with $x_2(t)$ if $\delta_{12}(t^+) > 0$, or the actual joining if $\delta_{12}(t^+) = 0$.
4. $C2O_i$: $G_i(t)$ switches from 1 (Closed switch) to 0 (Open switch).
5. $O2C_i$: $G_i(t)$ switches from 0 (Open switch) to 1 (Closed switch).

We can now identify the event set that affects the dynamics of the three queue content processes:

$$\begin{aligned} \Phi_1 &= \{S_1, E_1, O2C_1, C2O_1\} \\ \Phi_2 &= \{S_2, E_2, O2C_2, C2O_2, J_k\}, \\ \Phi_{12} &= \{S_{12}, E_{12}, E_1, C2O_1, J_k\} \end{aligned} \tag{13}$$

Table 1 List of frequently used notation

$x_i(t)$	Queue length of road i
$\bar{x}_2(t)$	the *estimate* of $x_2(t)$ based on the assumption that $x_2(t)$ is constant
$\delta_{12}(t)$	the distance between the head of the flow burst and the tail of i
$\alpha_i(t)$	incoming flow process
$\beta_i(t)$	outgoing flow process
$h_i(t)$	instantaneous outgoing flow rate
$G_i(t)$	switching controller of an outgoing flow
$z_i(t)$	clock state variable for switching controller i
J_k	a potential joining event of the flow burst with the downstream queue
σ_k	the event time of J_k with the downstream node
θ_i	controllable parameters

Note that this SFM model can be extended to any network of queues with possible delays by identifying queues with dynamics of type (1) or (6) or (5). Finally, to facilitate readability in what follows, we summarize in Table 1 all frequently used notation.

3 Multi-intersection traffic light control with delays

An application of the SFM with delays arises in the Traffic Light Control (TLC) problem in transportation networks, which consists of adjusting green and red signal settings in order to control the traffic flow through an intersection and, more generally, through a set of intersections and traffic lights in an urban roadway network. The ultimate objective is to minimize congestion in an area consisting of multiple intersections. Many methods have been proposed to solve the TLC problem, including expert systems, genetic algorithms, reinforcement learning and several optimization techniques; a more detailed review of such methods may be found in Fleck et al. (2016). Perturbation analysis methods were used in Head et al. (1996) and Fu and Howell (2003). IPA was used in Panayiotou et al. (2005) and Geng and Cassandras (2012) for a single intersection and extended to multiple intersections in Geng and Cassandras (2015) and to quasi-dynamic control schemes in Fleck et al. (2016). However, all this work to date has assumed that vehicles moving from one intersection to the next experience no delay. In this section, we formulate the TLC problem by including delays as in Section 2 and derive an IPA-based controller to optimize selected performance metrics (cost functions). By including delays, we will see that we can define new metrics which capture "congestion" in traffic systems much more accurately.

As in Section 2, let $\{\alpha_i(t)\}$ and $\{\beta_i(t)\}$, $i = 1, \ldots, 4$, be the incoming and outgoing flow processesrespectively at all four roads shown in Fig. 4, where we now interpret $\alpha_i(t)$ as the random instantaneous vehicle arrival rate at time t. We define the controllable parameters θ_i to be the durations of the GREEN light for road $i = 1, \ldots, 4$. Thus, the state vector

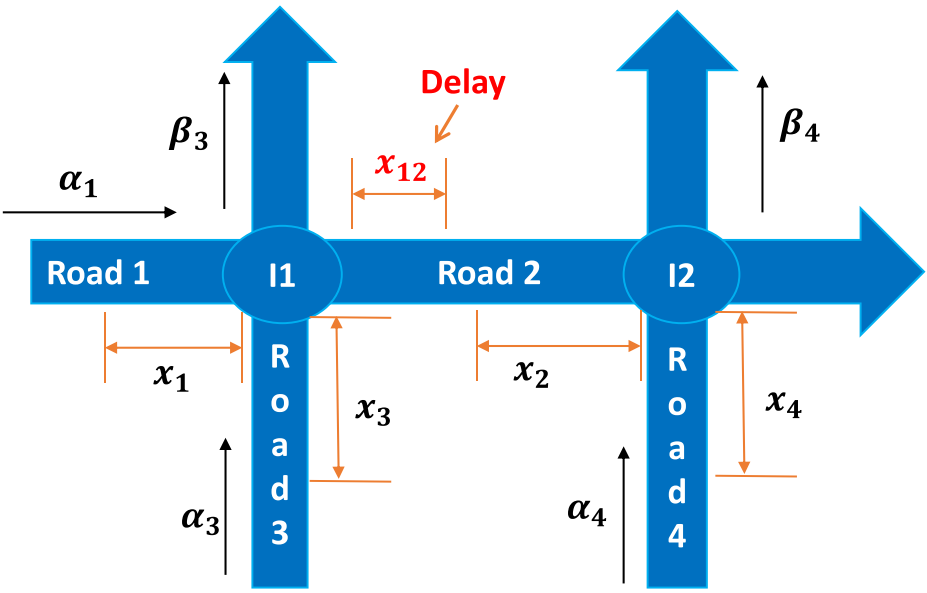

Fig. 4 Two traffic intersections

is $x(\theta,t) = [x_1(\theta,t), x_2(\theta,t), x_3(\theta,t), x_4(\theta,t), x_{12}(\theta,t)]$ where $x_i(\theta,t)$ is the content of queue i and $x_{12}(\theta,t)$ is the content of the road between intersections $I1$ and $I2$. To maintain notational simplicity, we will assume in our analysis that (**A1**) There is no more than one traffic burst in queue 12 at any one time, (**A2**) The speed of a traffic burst $v_1(t)$ between intersections is constant, and (**A3**) There is no traffic coupling between $I1$ and $I2$. Assumptions (**A1**) and (**A2**) simplify the analysis and can be easily relaxed since our model can deal with multiple flow bursts as shown in Section 2. Assumption (**A3**) means that the distance between $I2$ and $I1$ is sufficiently large and is also made to simplify the model; this assumption will be relaxed in Section 5.

We define clock state variables $z_i(t), i = 1,\ldots,4$, which are associated with the GREEN light cycle for queue i based on Eq. 3 where the controller $G_i(t)$ is now the traffic light state, i.e., $G_i(t) = 0$ means that the traffic light in road i is RED, otherwise, it is GREEN. Accordingly, the departure rates and the queue content dynamics $x_i(t)$, $i = 1,\ldots,4$, are given by Eqs. 1-6.

In order to provide the dynamics of $x_2(t)$ and $x_{12}(t)$, we will make use of our analysis in Section 2. In particular, let σ_0 be the time when a positive traffic flow is generated from queue 1 and enters queue 12, i.e., the light turns from RED to GREEN for road 1 and $x_1(\sigma_0) > 0$. Invoking (8), we define $\delta_{12}(t)$ to be the distance between the head of the "transit queue" 12 and the tail of queue 2. Thus, $\delta_{12}(\sigma_0^+) = L - x_2(\sigma_0)$. We also associate a clock to this queue, denoted by $z_{12}(t)$, which is defined by Eq. 7 and initialized at $z_{12}(\sigma_0) = 0$. Finally, $\tau(\delta_{12}(t))$ in Eq. 7 in the TLC context is given by $\tau(\delta_{12}(t)) = \delta_{12}(t)/v_1$.

Recall that a J_k event represents a *potential* joining of the flow burst from $I1$ with queue 2. The *actual* joining event occurs when $\delta_{12}(t^+) = 0$ from its initial value $\delta_{12}(\sigma_0^+) = L - x_2(\sigma_0)$. Adapting (8) and (4) to the TLC setting we get the dynamics of δ_{12} and $\bar{x}_2(t)$, while the dynamics of $x_2(t)$ and $x_{12}(t)$ are given by Eqs. 6 and 5 respectively.

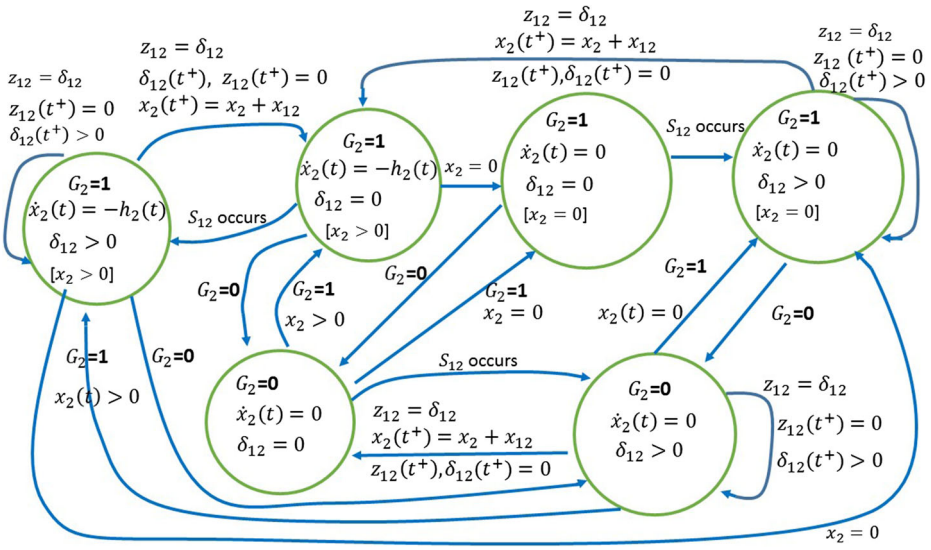

Fig. 5 Stochastic Hybrid Automaton model for $x_2(t)$

SFM Events We apply the event set defined in Section 2 where we use $G2R_i$ (traffic light i changes from GREEN to RED) to replace $C2O_i$ and $R2G_i$ to replace $O2C_i$. Thus, the set Φ_1 in Eq. 13 is used as Φ_i for $i = 1, 3, 4$ for the corresponding queues in Fig. 4. Figure 5 shows the hybrid automaton model for queue 2 in terms of its six possible modes depending on $x_2(t)$, $G_2(t)$ and $\delta_{12}(t)$. Similar models apply to the remaining processes, all of which are generally interdependent (e.g., in Fig. 5, some reset conditions involve $x_{12}(t)$).

Cost Functions The objective of the TLC problem is to control the green cycle parameters θ_i, $i = 1, \ldots, 4$, so as to minimize traffic congestion in the region covered by the two intersections in Fig. 4. In Geng and Cassandras (2012) and Fleck et al. (2016), the average total weighted queue length over a fixed time interval $[0, T]$ is used to capture congestion:

$$F(\theta; x(0), z(0), T) = \frac{1}{T} \sum_{i=1}^{5} \int_0^T w_i x_i(\theta, t) dt. \tag{14}$$

where w_i is the weight associated with queue i. For convenience, we will refer to Eq. 14 as the *average queue* cost function; with a slight abuse of notation we have re-indexed $x_{12}(t)$ as $x_5(t)$. However, this may not be an adequate measure of "congestion". For instance, it is possible that the average queue lengths over $[0, T]$ are relatively small, while reaching large values over small intervals (peak periods during a typical day). Thus, instead of restricting ourselves to Eq. 14, we define next two new cost functions.

1. *Average weighted Pth power of the queue lengths* over a fixed interval $[0, T)$, where $P > 1$. The sample function for this metric is

$$F(\theta; x(0), z(0), T) = \frac{1}{T} \sum_{i=1}^{5} \int_0^T w_i x_i^P(\theta, t) dt.$$

Observing that $x_i(\theta, t) = 0$ during an EP of queue i, we can rewrite this as

$$F(\theta; x(0), z(0), T) = \frac{1}{T} \sum_{i=1}^{5} \sum_{m=1}^{M_i} \int_{\xi_{i,m}}^{\eta_{i,m}} w_i x_i^P(\theta, t) dt, \tag{15}$$

in which M_i is the total number of NEPs of queue i over a time interval $[0, T]$ and $\xi_{i,m}$, $\eta_{i,m}$ are the occurrence times of the mth S_i event and E_i event respectively. We also define the cost incurred within the mth NEP of queue i as

$$F_{i,m}(\theta) = \int_{\xi_{i,m}}^{\eta_{i,m}} w_i x_i^P(\theta, t) dt. \tag{16}$$

Clearly, when $P = 1$, Eq. 15 is reduced to Eq. 14. When $P > 1$, Eq. 15 amplifies the presence of intervals where queue lengths are large. Therefore, minimizing Eq. 15 decreases the probability that a road develops a large queue length. We will refer to this metric Eq. 15 as the *power cost function.*

2. *Average weighted fraction of time that queue lengths exceed given thresholds* over a fixed interval $[0, T]$. The sample function for this metric is

$$\begin{aligned} F(\theta; x(0), z(0), T) &= \frac{1}{T} \sum_{i=1}^{5} \int_0^T w_i \mathbf{1}[x_i(\theta, t) > \zeta_i] dt \\ &= \frac{1}{T} \sum_{i=1}^{5} \int_0^T w_i r_i(\theta, t) dt \end{aligned} \tag{17}$$

where ζ_i is a given threshold and $r_i(\theta, t) = \mathbf{1}[x_i(\theta, t) > \zeta_i]$. This necessitates the definition of two additional events: Z_i is the event such that $x_i(\theta, t) = \zeta_i$, $x_i(\theta, t^-) < \zeta_i$ (i.e., the queue content reaches the threshold from below) and $\bar{Z}_i$ is the event such that $x_i(\theta, t) < \zeta_i$, $x_i(\theta, t^-) = \zeta_i$. Observe that $\dot{r}_i(\theta, t) = 0$ with a reset condition $r_i(\theta, t^+) = 1$ if $x_i(\theta, t^-) < \zeta_i$, $x_i(\theta, t^+) = \zeta_i$ and $r_i(\theta, t^+) = 0$ if $x_i(\theta, t^-) = \zeta_i$, $x_i(\theta, t^+) < \zeta_i$. Finally, we use $F_{i,m}(\theta)$ as in Eq. 16, for the cost associated with the mth NEP at queue i:

$$F_{i,m}(\theta) = \int_{\gamma_{i,m}(\theta)}^{\psi_{i,m}(\theta)} w_i r_i(\theta, t) dt. \tag{18}$$

where $\gamma_{i,m}$, $\psi_{i,m}$ are the start and end respectively of an interval such that $r_i(\theta, t) = 1$.

Optimization Our purpose is to minimize the cost functions defined in Eqs. 14, 15 and 17. We define the overall cost function as follows:

$$H(\theta; x(0), z(0), T) = E[F(\theta; x(0), z(0), T)],$$

in which $F(\theta; x(0), z(0), T)$ is a sample cost function of the form Eqs. 14 and 15 or Eq. 17. Clearly, we cannot derive a closed-form expression for the expectation above. However, we can estimate the gradient $\nabla H(\theta)$ through the sample gradient $\nabla F(\theta)$ based on IPA, which has been shown to be unbiased under mild technical conditions (Proposition 1 in Cassandras et al. 2010). We emphasize that *no explicit knowledge of* $\alpha_i(t)$ *and* $h_i(t)$ *is necessary* to estimate $\nabla H(\theta)$. The IPA estimators derived in the next section only need estimates of $\alpha_i(\tau_k)$ and $h_i(\tau_k)$ at certain event times τ_k. Using $\nabla F(\theta)$, we can use a simple gradient-descent optimization algorithm to minimize the associated cost metric through the iterative scheme

$$\theta_{j,k+1} = \theta_{j,k} - \mu_k Q_{j,k}(\theta_k, x(0), T, \omega_k),$$

in which $Q_{j,k}(\theta_k, x(0), T, \omega_k)$ is an estimator of $dH/d\theta_j$ (in our case, $dF/d\theta_j$) in sample path ω_k and μ_k is the step size at the kth iteration selected through an appropriate decreasing sequence to guarantee convergence (Fleck et al. 2016).

In the next section, we use the IPA methodology to obtain $dF/d\theta_j$ through the state derivatives $\frac{\partial x_i(\theta,t)}{\partial \theta_j}$.

4 Infinitesimal Perturbation Analysis (IPA)

We briefly review the IPA framework for general stochastic hybrid systems as presented in Cassandras et al. (2010). Let $\{\tau_k(\theta)\}$, $k = 1, \ldots, K$, denote the occurrence times of all events in the state trajectory of a hybrid system with dynamics $\dot{x} = f_k(x, \theta, t)$ over an interval $[\tau_k(\theta), \tau_{k+1}(\theta))$, where $\theta \in \Theta$ is some parameter vector and Θ is a given compact, convex set. For convenience, we set $\tau_0 = 0$ and $\tau_{K+1} = T$. We use the Jacobian matrix notation:

$$x'(t) \equiv \frac{\partial x(\theta, t)}{\partial \theta}, \qquad \tau_k' \equiv \frac{\partial \tau_k(\theta)}{\partial \theta}$$

for all state and event time derivatives. It is shown in Cassandras et al. (2010) that

$$\frac{d}{dt}x'(t) = \frac{\partial f_k(t)}{\partial x}x'(t) + \frac{\partial f_k(t)}{\partial \theta}, \tag{19}$$

for $t \in [\tau_k, \tau_{k+1})$ with boundary condition:

$$x'(\tau_k^+) = x'(\tau_k^-) + [f_{k-1}(\tau_k^-) - f_k(\tau_k^+)]\tau_k' \tag{20}$$

for $k = 1, ..., K$. In order to complete the evaluation of $x'(\tau_k^+)$ in Eq. 20, we need to determine τ_k'. If the event at τ_k is *exogenous* (i.e., independent of θ), then $\tau_k' = 0$. However, if the event is *endogenous*, there exists a continuously differentiable function $g_k : \mathbb{R}^n \times \Theta \to \mathbb{R}$ such that $\tau_k = \min\{t > \tau_{k-1} : g_k(x(\theta, t), \theta) = 0\}$ and, as long as $\frac{\partial g_k}{\partial x} f_k(\tau_k^-) \neq 0$,

$$\tau_k' = -\left[\frac{\partial g_k}{\partial x} f_k(\tau_k^-)\right]^{-1}\left[\frac{\partial g_k}{\partial \theta} + \frac{\partial g_k}{\partial x}x'(\tau_k^-)\right] \tag{21}$$

In our TLC setting, we will use the notation

$$x_{i,j}'(t) = \frac{\partial x_i(\theta, t)}{\partial \theta_j}, \quad z_{i,j}'(t) = \frac{\partial z_i(\theta, t)}{\partial \theta_j}, \quad \tau_{k,j}'(t) = \frac{\partial \tau_k(\theta)}{\partial \theta_j}$$

We also note that in Eqs. 1 and 5, $\frac{\partial f_k(t)}{\partial \theta} = \frac{\partial f_k(t)}{\partial x} = 0$ and Eq. 19 reduces to

$$x_{i,j}'(t) = x_{i,j}'(\tau_k^+), \quad t \in (\tau_k, \tau_{k+1}] \tag{22}$$

4.1 State and event time derivatives

We will now apply the IPA (20)-(22) to our TLC setting on an event by event basis for each of the events sets Φ_i, $i = 1, \ldots, 4$, and Φ_{12}. In all cases, τ_k denotes the associated event time.

4.1.1 IPA for Event Set $\Phi = \{,, 2, 2\} \cup \{,\}$, $= 1, 3, 4$

IPA for these three processes for each of the events in the first set above is identical to that in Geng and Cassandras (2012). Thus, we simply summarize the results here.

(1) *Event* E_i: $x'_{i,j}(\tau_k^+) = 0$.

(2) *Event* $G2R_i$: Let ρ_k be the time of the last $R2G_i$ event before $G2R_i$ occurs. Then, $\tau'_{k,j} = \mathbf{1}[j = i] + \rho'_{k,j}$ and

$$x'_{i,j}(\tau_k^+) = \begin{cases} x'_{i,j}(\tau_k) - \alpha_i(\tau_k)\tau'_{k,j} & \text{if } x_i(\tau_k) = 0,\ \alpha_i(\tau_k) \le \beta_i(\tau_k) \\ x'_{i,j}(\tau_k) - h_i(\tau_k)\tau'_{k,j} & \text{otherwise} \end{cases} \tag{23}$$

(3) *Event* $R2G_i$: Let ρ_k be the time of this event and τ_k be the time of the last $G2R_i$ event before $R2G_i$ occurs. We will use the notation $\hat{\imath}$ to denote the index of a road perpendicular to i (e.g., $\hat{1} = 3, \hat{2} = 4$ in Fig. 4). Then, $\rho'_{k,j} = \mathbf{1}[j = \hat{\imath}] + \tau'_{k,j}$ and

$$x'_{i,j}(\rho_k^+) = \begin{cases} x'_{i,j}(\rho_k) + \alpha_i(\rho_k)\rho'_{k,j} & \text{if } x_i(\rho_k) = 0,\ \alpha_i(\rho_k) \le \beta_i(\rho_k) \\ x'_{i,j}(\rho_k) + h_i(\rho_k)\rho'_{k,j} & \text{otherwise} \end{cases} \tag{24}$$

(4) *Event* S_i: If S_i is induced by $G2R_i$, then $x'_{i,j}(\tau_k^+) = x'_{i,j}(\tau_k) - \alpha_i(\tau_k)\tau'_{k,j}$. If S_i is an exogenous event triggered by Γ_i , then $x'_{12,j}(\tau_k^+) = x'_{12,j}(\tau_k)$.

For the two new events $\{Z_i, \bar{Z}_i\}$, we have:

(5) *Event* Z_i: This is an endogenous event which occurs when $g_k(x(\theta,t),\theta) = x_i(\tau_k) - \zeta_i = 0$. Applying (21), we have

$$\tau'_{k,j} = \begin{cases} -x'_{i,j}(\tau_k)/\alpha_i(\tau_k) & \text{if } G_i(\tau_k) = 0 \\ -x'_{i,j}(\tau_k)/[\alpha_i(\tau_k) - h_i(\tau_k)] & \text{if } G_i(\tau_k) = 1 \end{cases} \tag{25}$$

Moreover, based on the definition $r_i(t) = \mathbf{1}[x_i(t) > \zeta_i]$ in Section 3, $r_i(\tau_k^+) = 1$, which implies that $r'_{i,j}(\tau_k^+) + \dot{r}(\tau_k^+)\tau_{k,j}^+ = 0$. Since $\dot{r}_i(\tau_k^+) = 0$, we get $r'_{i,j}(\tau_k^+) = 0$.

(6) *Event* $\bar{Z}_i$: Similar to the previous case, $g_k(x(\theta,t),\theta) = x_i(\tau_k) - \zeta_i = 0$ and applying (21) gives

$$\tau'_{k,j} = -x'_{i,j}(\tau_k)/(\alpha_i(\tau_k) - h_i((\tau_k))) \tag{26}$$

In this case, $r_i(\tau_k^+) \equiv 0$, therefore, $r'_{i,j}(\tau_k^+) + \dot{r}_i(\tau_k^+)\tau_{k,j}^+ = 0$ and, since $\dot{r}_i(\tau_k^+) = 0$, we get $r'_{i,j}(\tau_k^+) = 0$.

4.1.2 IPA for Event Set $\Phi_2 = \{2, 2, 2_2, 2_2, \} \cup \{2, \bar{2}\}$

Applying IPA for this set and for Φ_{12} leads to new derivative estimators as detailed next.

(1) *Event* E_2: This is an endogenous event ending an EP that occurs when $g_k(x(\theta,t),\theta) = x_2(t) = 0$ at $t = \tau_k$. Applying (21) and using Eq. 6, we have $\tau'_{k,j} = x'_{2,j}(\tau_k^-)/h_2(\tau_k^-)$. It then follows from Eq. 20 that $x'_{2,j}(\tau_k^+) = x'_{2,j}(\tau_k^-) - h_2(\tau_k^-)\tau'_{k,j} = 0$.

(2) *Event* S_2: In view of the reset condition in Eq. 6, this event is induced by J_k provided $\delta_{12}(t^+) = 0$. As described in Section 2, a sequence of J_k events is initiated when a flow burst is generated at node 1 with associated event times $\{\sigma_0, \sigma_1, \ldots, \sigma_K\}$. Event S_2 is induced by the last occurrence of a J_k event at time σ_K. Thus, our goal here is to evaluate the IPA derivative $x'_{2,j}(\sigma_K^+)$. At first sight, it would appear that this requires the complete sequence $\{x'_{2,j}(\sigma_0^+), \ldots, x'_{2,j}(\sigma_{K-1}^+)\}$ along with event time

derivatives $\{\sigma'_{0,j}, \ldots, \sigma'_{K-1,j}\}$ from which $x'_{2,j}(\sigma_K^+)$ can be inferred. However, the following lemma shows that the only information needed from the full sequence of J_k events is σ'_0.

Lemma 2 *Let σ_k, $k = 0, 1, \ldots, K$ be the occurrence time of event J_k for a flow burst initiated at σ_0. Then,*

$$\sigma'_{k,j} = \frac{-1}{v_1}[x'_{2,j}(\sigma_{k-1}) + \dot{x}_2(\sigma_{k-1})\sigma'_{k-1,j}] + \sigma'_{0,j}$$

Proof Event J_k at $t = \sigma_k$ is endogenous and occurs when $g_k(x(\theta, \sigma_k), \theta) = z_{12}(\sigma_k) - \delta_{12}(\sigma_k)/v_1 = 0$. Applying (21) and using Eqs. 7 and 8, we get $\sigma'_{k,j} = \delta'_{12,j}(\sigma_k)/v_1 - z'_{12,j}(\sigma_k)$. Using Eq. 22, we have $\delta'_{12,j}(\sigma_k) = \delta'_{12,j}(\sigma_{k-1}^+)$ and it follows that

$$\sigma'_{k,j} = \delta'_{12,j}(\sigma_{k-1}^+)/v_1 - z'_{12,j}(\sigma_k) \tag{27}$$

Again applying (22) gives $z'_{12,j}(\sigma_k) = z'_{12,j}(\sigma_{k-1}^+)$. From Eq. 20, in view of Eq. 7, we get, for $k = 1$, $z'_{12,j}(\sigma_0^+) = -\sigma'_{0,j}$. The reset condition in Eq. 8 implies that $\delta_{12}(\sigma_0^+) = L - x_2(\sigma_0)$, hence $\delta'_{12,j}(\sigma_0^+) = -x'_{2,j}(\sigma_0) - \dot{x}_2(\sigma_0)\sigma'_{0,j}$. Thus, in this case, Eq. 27 gives:

$$\sigma'_{1,j} = \frac{-1}{v_1}[x'_{2,j}(\sigma_0) + \dot{x}_2(\sigma_0)\sigma'_{0,j}] + \sigma'_{0,j} \tag{28}$$

For $k > 1$, based on the reset condition in Eq. 7, we have $z_{12}(\sigma_k^+) = 0$. Taking the total derivative, we get $z'_{12,j}(\sigma_k^+) = -\sigma'_{k,j}$. The reset condition in Eq. 8 now implies that $\delta_{12}(\sigma_{k-1}^+) = \bar{x}_2(\sigma_{k-1}) - x_2(\sigma_{k-1})$, hence

$$\begin{aligned}\delta'_{12,j}(\sigma_{k-1}^+) &= \bar{x}'_{2,j}(\sigma_{k-1}) + \dot{\bar{x}}_2(\sigma_{k-1})\sigma'_{k-1,j} \\ &\quad -x'_{2,j}(\sigma_{k-1}) - \dot{x}_2(\sigma_{k-1})\sigma'_{k-1,j}\end{aligned} \tag{29}$$

Applying (22), we have $\bar{x}'_{2,j}(\sigma_{k-1}) = \bar{x}'_{2,j}(\sigma_{k-2}^+)$. Looking at Eq. 4, we have $\dot{\bar{x}}_2(\sigma_{k-1}) = 0$ and the reset condition implies that $\bar{x}'_{2,j}(\sigma_{k-2}^+) = x'_{2,j}(\sigma_{k-2}) + \dot{x}_2(\sigma_{k-2})\sigma'_{k-2,j}$. Thus, returning to Eq. 29, we get

$$\begin{aligned}\delta'_{12,j}(\sigma_{k-1}^+) &= x'_{2,j}(\sigma_{k-2}) + \dot{x}_2(\sigma_{k-2})\sigma'_{k-2,j} \\ &\quad -x'_{2,j}(\sigma_{k-1}) - \dot{x}_2(\sigma_{k-1})\sigma'_{k-1,j}\end{aligned} \tag{30}$$

Recalling that $z'_{12,j}(\sigma_k^+) = -\sigma'_{k,j}$ and combining (28), (30) into (27), we get

$$\begin{aligned}\sigma'_{k,j} &= \sigma'_{k-1,j} + \frac{1}{v_1}[x'_{2,j}(\sigma_{k-2}) + \dot{x}_2(\sigma_{k-2})\sigma'_{k-2,j} - x'_{2,j}(\sigma_{k-1}) - \dot{x}_2(\sigma_{k-1})\sigma'_{k-1,j}] \\ &= \sigma'_{0,j} + \frac{1}{v_1}[-x'_{2,j}(\sigma_{k-1}) - \dot{x}_2(\sigma_{k-1})\sigma'_{k-1,j}]\end{aligned} \tag{31}$$

where the last step follows from a recursive evaluation of $\sigma'_{k-1,j}$ using Eqs. 28 and 31 leading to the cancellation of many of the terms above. This completes the proof. □

Let us now focus on event J_K at time σ_K. It follows from the reset condition in Eq. 6 that

$$x'_{2,j}(\sigma_K^+) = \begin{cases} x'_{2,j}(\sigma_K) + x'_{12,j}(\sigma_K) & \text{if } G_2(\sigma_K) = 1 \\ +h_2(\sigma_K^+)\sigma'_{K,j} & \text{and } x_2(\sigma_K) = 0 \\ x'_{2,j}(\sigma_K) + x'_{12,j}(\sigma_K) & \text{otherwise} \end{cases} \tag{32}$$

Recall that $\delta_{12}(\sigma_K^+) = 0$ in Eq. 32. If $G_2(\sigma_K) = 1$ and $x_2(\sigma_K) = 0$, then $x_2(\sigma_{K-1}) - x_2(\sigma_K) = 0$, hence $x_2(\sigma_{K-1}) = 0$. It follows from Eqs. 6 and 8 that $\dot{x}_2(\sigma_{K-1}) = 0$. Based on Case **1** above, we get $x'_{2,j}(\sigma_{K-1}) = 0$. Then, from Lemma 2, $\sigma'_{K,j} = \sigma'_{0,j}$ and Eq. 32 becomes

$$x'_{2,j}(\sigma_K^+) = \begin{cases} x'_{2,j}(\sigma_K) + x'_{12,j}(\sigma_K) & \text{if } G_2(\sigma_K) = 1 \\ +h_2(\sigma_K^+)\sigma'_{0,j} & \text{and } x_2(\sigma_K) = 0 \\ x'_{2,j}(\sigma_K) + x'_{12,j}(\sigma_K) & \text{otherwise} \end{cases} \tag{33}$$

We conclude that the state derivative $x'_{2,j}(\sigma_K^+)$ when event S_2 occurs is independent of all event time derivatives $\sigma'_{1,j}, \ldots, \sigma'_{K,j}$ and involves only $\sigma'_{0,j}$, evaluated when the associated flow burst is initiated.

(3) *Event* $G2R_2$: This is an endogenous event that occurs when $g_k(x(\theta,t),\theta) = z_2(t) - \theta_2 = 0$. Based on Eq. 21, $\tau'_{k,j} = \mathbf{1}[j=2] - z'_{2,j}(\tau_k)$. Let ρ_k be the last $R2G_2$ before $G2R_2$ occurs. Applying (22), we have $z'_{2,j}(\rho_k^+) = z'_{2,j}(\tau_k)$, and from Eq. 20 we get $z'_{2,j}(\rho_k^+) = -\rho'_{k,j}$. It follows that $\tau'_{k,j} = \mathbf{1}[j=2] + \rho'_{k,j}$. Based on Eq. 20, we have

$$x'_{2,j}(\tau_k^+) = \begin{cases} x'_{2,j}(\tau_k) - h_2(\tau_k)\tau'_{k,j} & \text{if } x_2(\tau_k) > 0 \\ x'_{2,j}(\tau_k) & \text{otherwise} \end{cases} \tag{34}$$

(4) *Event* $R2G_2$*:* Let ρ_k be the time of this event and τ_k be the time of the last $G2R_2$ event before $R2G_2$ occurs. Similar to **(3)** above, we get $\rho'_{k,j} = \mathbf{1}[j=4] + \tau'_{k,j}$ and use this value in the expression below which follows from Eq. 20:

$$x'_{2,j}(\rho_k^+) = \begin{cases} x'_{2,j}(\rho_k) + h_2(\tau_k^+)\rho'_{k,j} & \text{if } x_2(\rho_k) > 0 \\ x'_{2,j}(\rho_k) & \text{otherwise} \end{cases} \tag{35}$$

(5) *Event* J_k: The analysis of this event has already been done in Case **(2)** above, including Lemma 2**.**

(6) *Event* Z_2: This is an endogenous event which is triggered by J_k: if a traffic burst from node 1 joins $x_2(t)$ at $t = \tau_k$ and $x_2(\tau_k^+) > \zeta_2$, this results in Z_2. Since $r_2(\tau_k^+) = 1$ and $\dot{r}_2(t) = 0$, we have $r'_{2,j}(\tau_k^+) = 0$.

(7) *Event* $\bar{Z}_2$: This is an endogenous event that occurs when $g_k(x(\theta,t),\theta) = x_2(\theta,t) - \zeta_2 = 0$. Applying (21), we have $\tau'_{k,j} = x'_2(\tau_k)/h_2(\tau_k)$. Moreover, $r_2(\tau_k^+) \equiv 0$, therefore, $r'_{2,j}(\tau_k^+) + \dot{r}_2(\tau_k^+)\tau'_{k,j} = 0$ and, since $\dot{r}_2(\tau_k^+) = 0$, we get $r'_{2,j}(\tau_k^+) = 0$.

4.1.3 IPA for event set $\Phi_{12} = \{_{12}, _{12}, _1, 2_1, \} \cup \{_{12}, \bar{}_{12}\}$

(1) *Event* S_{12}: This event can be either exogenous or endogenous. If $x_1(\tau_k) > 0$ or if $x_1(\tau_k) = 0$, $\alpha_1(t) > 0$, S_{12} is induced by event $R2G_1$ which is endogenous. Otherwise, S_{12} is an exogenous event and occurs when $G_1(\tau_k) = 1$ and $\alpha_1(\tau_k)$ switches from zero to some positive value.

Case (1a) *S_{12} is induced by $R2G_1$.* Referring to our analysis of $R2G_1$ (Case **(3)** for Φ_1), we have already evaluated $\tau'_{k,j}$. Then, applying (20), we get

$$x'_{12,j}(\tau_k^+) = \begin{cases} x'_{12,j}(\tau_k) - \alpha_1(\tau_k^+)\tau'_{k,j} & \text{if } x_1(\tau_k) = 0 \text{ and} \\ & 0 < \alpha_1(\tau_k) \le \beta_1(\tau_k) \\ x'_{12,j}(\tau_k) - h_1(\tau_k^+)\tau'_{k,j} & \text{otherwise} \end{cases} \tag{36}$$

Case (1b) *S_{12} is exogenous*. In this case, $\tau'_{k,j} = 0$ and applying (20) gives $x'_{12,j}(\tau_k^+) = x'_{12,j}(\tau_k)$.

(2) *Event E_{12}*: This event occurs when the traffic burst in queue 12 joins queue 2. This is an endogenous event that occurs when $g_k(x(\theta,\tau_k),\theta) = z_{12}(\tau_k) - \delta_{12}(\tau_k) = 0$ and $\delta_{12}(\tau_k^+) = 0$. When this happens, it follows from the reset condition in Eq. 5 that $x'_{12,j}(\tau_k^+) = 0$.

(3) *Event E_1*: This is an endogenous event that occurs when $g_k(x(\theta,t),\theta) = x_1(t) = 0$. Applying (21), we get $\tau'_{k,j} = -\frac{x'_{1,j}(\tau_k)}{\alpha_1(\tau_k)-h_1(\tau_k)}$. Thus, using Eq. 20, we get

$$\begin{aligned} x'_{12,j}(\tau_k^+) &= x'_{12,j}(\tau_k) + (h_1(\tau_k) - \alpha_1(\tau_k))\tau'_{k,j} \\ &= x'_{12,j}(\tau_k) + x'_{1,j}(\tau_k) \end{aligned} \tag{37}$$

(4) *Event $G2R_1$*: This is an endogenous event that occurs when $g_k(x(\theta,t),\theta) = z_1(t) - \theta_1 = 0$. It was shown under the analysis for events in Φ_1 that for $G2R_1$ we have $\tau'_{k,j} = \mathbf{1}[j=i] + \rho'_{k,j}$ where ρ_k is the time of the last $R2G_1$ event before $G2R_1$ occurs. Using this value, we can evaluate the following which follows from Eq. 20:

$$x'_{12,j}(\tau_k^+) = \begin{cases} x'_{12,j}(\tau_k) + \alpha_1(\tau_k)\tau'_{k,j} & \text{if } x_1(\tau_k) = 0 \\ & \text{and } \alpha_1(\tau_k) \le \beta_1(\tau_k) \\ x'_{12,j}(\tau_k) + h_1(\tau_k)\tau'_{k,j} & \text{otherwise} \end{cases} \tag{38}$$

(5) *Event J_k*: The analysis of this event has already been done in Case **(2)** above, including Lemma 2**.**

(6) *Event Z_{12}*: This is an endogenous event that occurs when $g_k(x(\theta,t),\theta) = x_{12}(\theta,t) - \zeta_{12} = 0$. Applying (21), we have

$$\tau'_{k,j} = \begin{cases} -\frac{x'_{12,j}(\tau_k)}{\alpha_1(\tau_k)} & \text{if } x_1(\tau_k) = 0 \\ & \text{and } \alpha_1(\tau_k) \le \beta_1(\tau_k) \\ -\frac{x'_{12,j}(\tau_k)}{h_1(\tau_k)} & \text{otherwise} \end{cases}$$

Since $r_{12}(\tau_k^+) = 1$ and $\dot{r}_{12}(t) = 0$, we have $r'_{12,j}(\tau_k^+) = 0$.

(7) *Event $\bar{Z}_{12}$*: This is triggered by event E_{12} when the traffic burst in queue 12 joins queue 2 and we reset $x_{12}(\tau_k^+) = 0$. Since $r_{12}(\tau_k^+) = 0$ and $\dot{r}_{12}(t) = 0$, we have $r'_{12,j}(\tau_k^+) = 0$.

4.2 Cost function derivatives

Returning to Eqs. 14, 15, and 17, recall that the IPA estimator consists of the gradient formed by the sample performance derivatives $\frac{\partial F}{\partial \theta_j}$, $j = 1,2,3,4$, which in turn depend on the state derivatives that we have evaluated in the previous section. The derivation of the IPA estimator for the Average Queue cost function in Eq. 14 is similar to that in Geng and Cassandras (2012) and related prior work and is omitted. Instead, we concentrate on the two new cost functions (15) and (17).

For the Power cost function, we derive $\frac{\partial F_{i,m}(\theta)}{\partial \theta_j}$ from Eq. 16, from which $\frac{\partial F}{\partial \theta_j}$ is obtained by adding over all M_i NEPs of each queue i over $[0, T]$:

$$\begin{aligned}\frac{\partial F_{i,m}(\theta)}{\partial \theta_j} &= P x_{i,j}^{'}(\theta,t)\int_{\xi_{i,m}(\theta)}^{\eta_{i,m}(\theta)} w_i x_i^{P-1}(\theta,t)dt \\ &= P[x_{i,j}^{'}(\xi_{i,m}^{+})\int_{\xi_{i,m}(\theta)}^{t_{i,m}^{1}} w_i x_i^{P-1}(\theta,t)dt \\ &\quad + \sum_{j=2}^{J_{i,m}} x_{i,j}^{'}((t_{i,m}^{j})^{+})\int_{t_{i,m}^{j-1}}^{t_{i,m}^{j}} w_i x_i^{P-1}(\theta,t)dt \\ &\quad + x_{i,j}^{'}((T_{i,m})^{+})\int_{T_{i,m}}^{\eta_{i,m}} w_i x_i^{P-1}(\theta,t)dt],\end{aligned}$$

where $t_{i,m}^{j}$, $j = 1, ..., J_{i,m}$ is the occurrence time of the jth event in the mth NEP of queue i and $t_{i,m}^{J_{i,m}}$ is simplified as $T_{i,m}$. The state derivative is determined on an event-driven basis using $x_{i,j}^{'}(\tau_k^{+})$ corresponding to the event occurring at time τ_k; for instance, if $G2R_1$ occurs at node 1, then Eq. 23 is invoked with $i = 1$.

For the Threshold cost function, we know that $r^{'}(\theta,t) = 0$ and it follows from Eq. 18:

$$\begin{aligned}\frac{\partial F_{i,m}(\theta)}{\partial \theta_j} &= \int_{\gamma_{i,m}(\theta)}^{\psi_{i,m}(\theta)} w_i r_{i,j}^{'}(\theta,t)dt - w_i r_i(\theta,\gamma_{i,m}^{+})\gamma_{i,m,j}^{'} + w_i r_i(\theta,\psi_{i,m}^{-})\psi_{i,m,j}^{'} \\ &= w_i(\psi_{i,m,j}^{'} - \gamma_{i,m,j}^{'}),\end{aligned}$$

Note that in this case the derivative depends only on $\psi_{i,m,j}^{'}$, $\gamma_{i,m,j}^{'}$, the event time derivatives in Eqs. 25 and 26 for $i = 1, 3, 4$ and the corresponding event time derivatives in Cases **(6), (7)** for each of sets Φ_{22} and Φ_{12}.

5 TLC with blocking between intersections

In this section, we relax the assumption made in Chen and Cassandras (2018) to include blocking effects between intersections. Therefore, we allow for the possibility that the length of the road between two intersections is sufficiently short so that traffic backlog can fill this space up when the incoming traffic flow is large or the green traffic light duration at the downstream intersection is too short. In our modified model, we impose the constraint $x_2(t) \leq L$. Due to this constraint, there are two new events:

1. $B2U$: $x_2(t)$ switches from the blocking state ($x_2(t) = L$) to the unblocked state ($x_2(t) < L$).
2. $U2B$: $x_2(t)$ switches from the unblocked state ($x_2(t) < L$) to the blocking state ($x_2(t) = L$).

Figure 6 shows how the blocking state ($x_2(t) = L$) introduces new modes for the dynamics of $x_1(t)$ and $x_2(t)$. In addition to the modes of $x_1(t)$ in Eq. 1 and of $x_2(t)$ in Eq. 5, additional modes to these dynamics are added as follows:

$$\dot{x}_1(t) = \begin{cases} \alpha_1(t) - \beta_2(t) & \text{if } x_2(t) = L, G_2(t) = 1 \\ \alpha_1(t) & \text{if } x_2(t) = L, G_2(t) = 0 \end{cases} \tag{39}$$

$$\dot{x}_2(t) = 0 \text{ if } x_2(t) = L \tag{40}$$

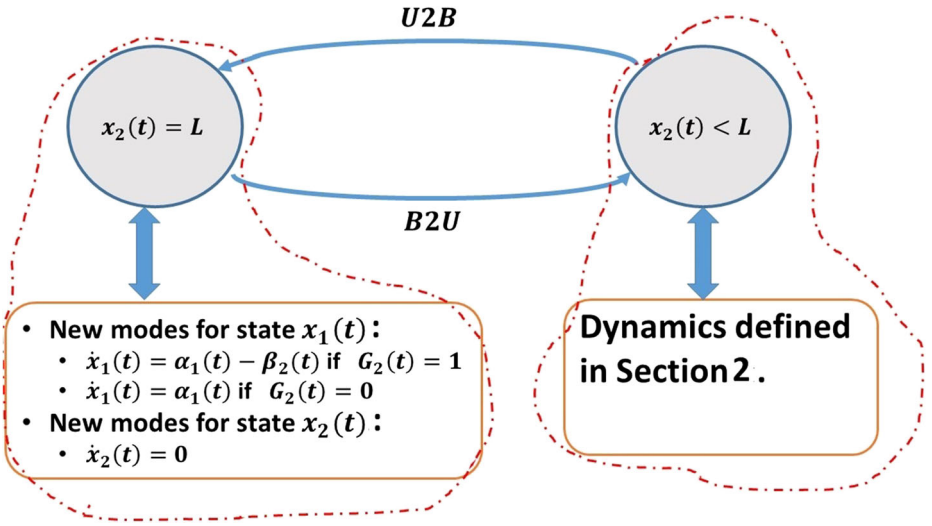

Fig. 6 Traffic Blocking for $x_2(t)$

Events $B2U$ and $U2B$ only influence the dynamics of $x_1(t)$ and $x_2(t)$. Since IPA is driven by the events affecting the state dynamics, we update the event sets Φ_1 and Φ_2 as follows and then provide the corresponding IPA derivative estimates:

$$\Phi_1 = \{S_1, E_1, R2G_1, G2R_1\} \cup \{U2B, B2U\}$$
$$\Phi_2 = \{S_2, E_2, R2G_2, G2R_2, J_k\} \cup \{U2B, B2U\}$$

5.1 *IPA for Event Set* $\{1, 1, 2_1, 2_1\} \cup \{2, 2\}$

Except for the new events $U2B$ and $B2U$, the IPA derivative estimates for all other events in Φ_1 are the same as in Section 4. Therefore, we only consider how $x'_{1,j}$, $j = 1, \ldots, 4$, are affected by these events.

(1) *Event* $U2B$: This can only be triggered by event J_k. When a flow burst joins $x_2(t)$, it is possible that $x_2(t) = L$. The guard condition ensuring $U2B$ is triggered by J_k is $x_{12}(t) + x_2(t) = L$ when J_k occurs at time $t = \tau_k$. It follows from the dynamics of $x_1(t)$ that

$$x'_{1,j}(\tau_k^+) = \begin{cases} x'_{1,j}(\tau_k) - \beta_1(\tau_k)\tau'_{k,j} & \text{if } G_2(\tau_k) = 0, x_1(\tau_k) > 0 \\ x'_{1,j}(\tau_k) - \alpha_1(\tau_k)\tau'_{k,j} & \text{if } G_2(\tau_k) = 0, x_1(\tau_k) = 0 \\ x'_{1,j}(\tau_k) & \\ +(\beta_2(\tau_k) - \beta_1(\tau_k))\tau'_{k,j} & \text{if } G_2(\tau_k) = 1, x_1(\tau_k) > 0 \\ x'_{1,j}(\tau_k) & \\ +(\beta_2(\tau_k) - \alpha_1(\tau_k))\tau'_{k,j} & \text{if } G_2(\tau_k) = 1, x_1(\tau_k) = 0 \end{cases} \tag{41}$$

(2) *Event* $B2U$: This event can be triggered by events which influence the incoming and outgoing flows of $x_2(t)$. We consider each of them as follows and provide the associated IPA state derivative.

(2a) *B2U is triggered by event $R2G_2$.* Guard conditions are needed for this case to be true, i.e., $x_1(t) > 0$, $\beta_2(t) > \beta_1(t)$ and $G_1(t) = 1$ or $G_1(t) = 0$. If $x_1(t) > 0$, $\beta_2(t) > \beta_1(t)$ and $G_1(t) = 1$, the outgoing flow from the downstream node 2 exceeds the incoming flow to node 2 from the upstream node 1 to decrease $x_2(t)$ when event $R2G_2$ occurs. If $G_1(t) = 0$, the outgoing flow from the downstream node 2 decreases $x_2(t)$ when event $R2G_2$ occurs since there is no incoming flow from node 1. Let τ_k be the event time of $R2G_2$ which was analyzed in Section 4.1. We have

$$x'_{1,j}(\tau_k^+) = \begin{cases} x'_{1,j}(\tau_k) + \beta_1(\tau_k)\tau'_{k,j} & \text{if } G_1(\tau_k) = 1, x_1(\tau_k) > 0 \text{ and } \beta_2(\tau_k) > \beta_1(\tau_k) \\ x'_{1,j}(\tau_k) & \text{otherwise} \end{cases} \tag{42}$$

(2b) *B2U is triggered by event $G2R_1$.* The guard condition for this case is $G_2(t) = 1$ which releases the traffic backlog from queue 2. Let τ_k be the event time of $G2R_1$ which was analyzed in Section 4.1. We have

$$x'_{1,j}(\tau_k^+) = x'_{1,j}(\tau_k) - \beta_2(\tau_k)\tau'_{k,j} \tag{43}$$

(2c) *B2U is triggered by event E_1.* The guard condition is $\alpha_1(t) - \beta_2(t) \leq 0$ and $G_2(t) = 1$. Since $x_1(t) = 0$, it is easy to show that $x'_{1,j}(\tau_k^+) = 0$.

(2d) *B2U is triggered by an event such that $\beta_1(t) - \beta_2(t)$ switches from a non-negative value to a negative value.* The guard condition is $x_1(t) > 0$ and $G_2(t) = 1$. Let τ_k be the associated event time. Since this event is exogenous, we must have $\tau'_k = 0$ which leads to $x'_{1,j}(\tau_k^+) = x'_{1,j}(\tau_k)$.

(2e) *B2U is triggered by an event such that $\alpha_1(t) - \beta_2(t)$ changes from a non-negative value to a negative value.* The guard conditions are $x_1(t) = 0$ and $G_2(t) = 1$. Along the same lines as **(2d)**, we have $x'_{1,j}(\tau_k^+) = 0$.

5.2 IPA for event set $\{_2, _2, 2_2, 2_2, \} \cup \{2, 2\}$

Since the IPA derivative evaluation for events $\{S_2, E_2, R2G_2, G2R_2, J_k\}$ is given in Section 4, we only consider here events $U2B$ and $B2U$ in the following.

(1) *Event $U2B$*: The analysis of this event was shown above. When this event occurs, we must have $x_2(t) = L$. Since $\dot{x}_2(t) = 0$, we have $x'_{2,j}(\tau_k^+) = 0$.

(2) *Event $B2U$*: Let τ_k be the event time of $B2U$. The analysis of this event is the same as that for $x_1(t)$ and omitted here. We derive only the state derivative $x'_{2,j}(\tau_k^+)$.

(2a) *B2U is triggered by event $R2G_2$.* It follows from the dynamics of $x_2(t)$ that

$$x'_{2,j}(\tau_k^+) = x'_{2,j}(\tau_k) + \beta_2(\tau_k)\tau'_{k,j}$$

(2b) *B2U is triggered by event $G2R_1$.* It follows from the dynamics of $x_2(t)$ that

$$x'_{2,j}(\tau_k^+) = x'_{2,j}(\tau_k) + \beta_2(\tau_k)\tau'_{k,j}$$

(2c) *B2U is triggered by event E_1.* We have

$$x'_{2,j}(\tau_k^+) = x'_{2,j}(\tau_k) + \beta_2(\tau_k)\tau'_{k,j}$$

(2d) *B2U is triggered by an event such that $\beta_1(t) - \beta_2(t)$ changes from a non-negative value to a negative value.* Since $\tau'_k = 0$, we have $x'_{2,j}(\tau_k^+) = x'_{2,j}(\tau_k)$.

(2e) *B2U is triggered by an event such that $\alpha_1(t) - \beta_2(t)$ changes from a non-negative value to a negative value.* We have $x'_{2,j}(\tau_k^+) = x'_{2,j}(\tau_k)$.

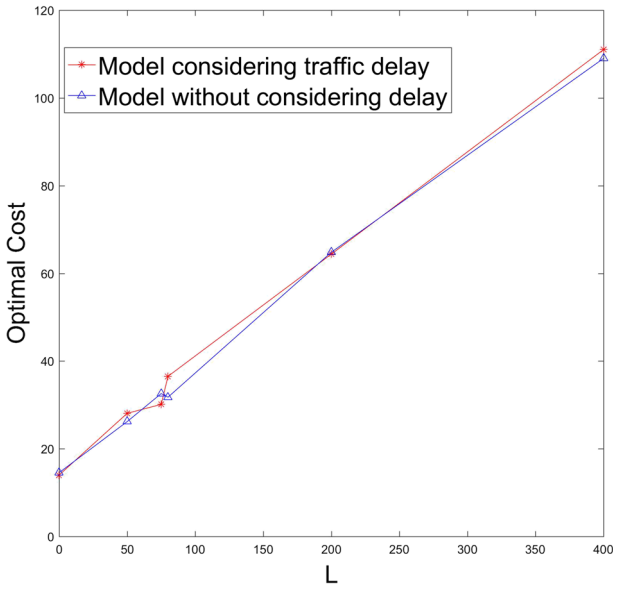

Fig. 7 Comparison of Optimal Average Queue Cost vs L

6 Simulation results

In this section, we use the derived IPA estimators in order to optimize the green light cycles in the two-intersection model of Fig. 4. We emphasize that this model is simulated as a Discrete Event System (DES) with individual vehicles rather than flows, so that the resulting estimators are based on *actual observed data*. This is made possible by the fact that all SFM events in the sets Φ_i, $i = 1, \ldots, 4$, and Φ_{12} coincide with those of the DES, therefore they are directly observable along with their occurrence times.

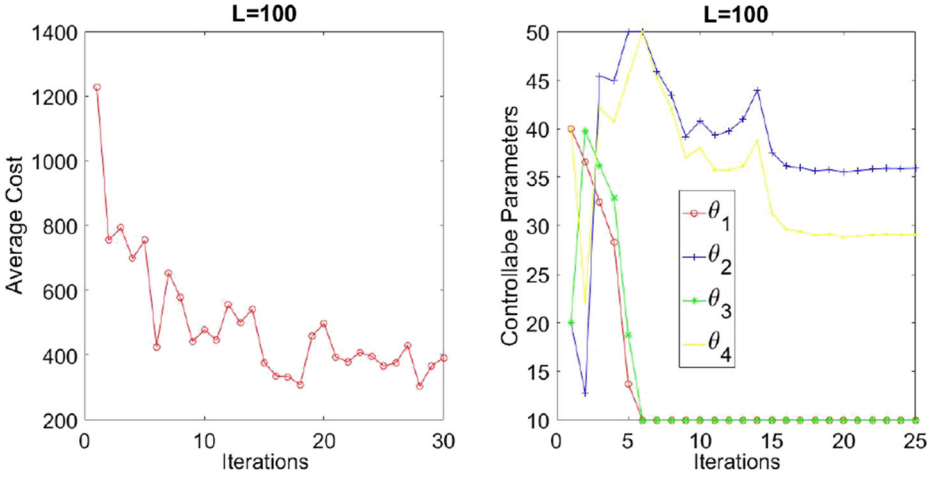

Fig. 8 Optimal Power Cost Function and Controllable Parameters vs Iterations

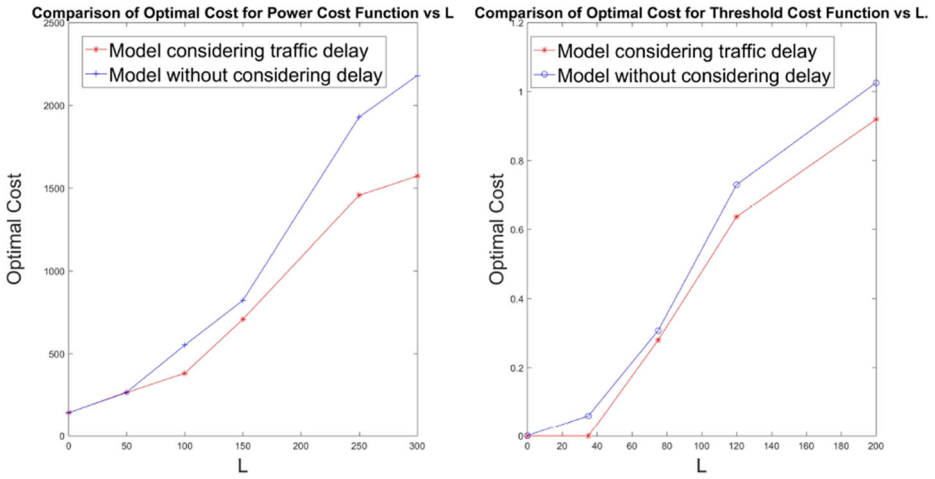

Fig. 9 Comparison of Optimal Power Cost with/without delay vs L

For simplicity, we assume that all vehicle arrival processes are Poisson (recall, however, that IPA is *independent of these distributions*) with rates $\tilde{\alpha_i}$, $i = 1, 3, 4$, and that the vehicle departure rate $h_i(t)$ on each non-empty road is constant. We also set the length of each vehicle as unit 1 which does not change the nature of TLC when we initiate L and queue length $x_i(t)$, $i = 1, 2, 3, 4, 12$. In Geng and Cassandras (2015), only one controllable parameter per intersection was considered by setting $\theta_i + \theta_{\hat{i}} = C$. Here, we relax this constraint. Moreover, we limit each controllable parameter so that $\theta_i \in [\theta_{i,min}, \theta_{i,max}]$ where $\theta_{i,min}$ and $\theta_{i,max}$ are given lower and upper bounds, respectively, for feasible green light cycle values. In our simulations, $\alpha_i(\tau_k)$ is estimated through N_a/t_w by counting the number of arriving vehicles N_a over a time window $[0, t_w]$ and $h_i(t)$ is estimated using the same method as in

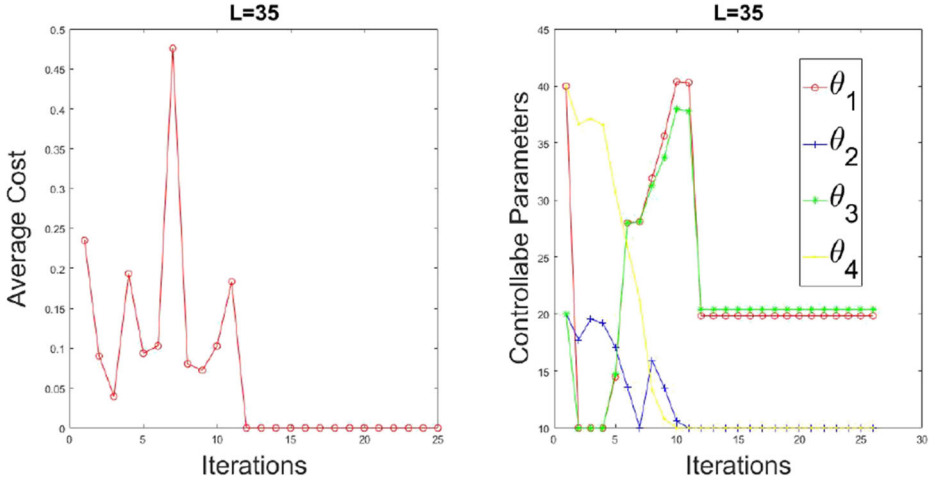

Fig. 10 Optimal Threshold Cost Function and Controllable Parameters vs Iterations

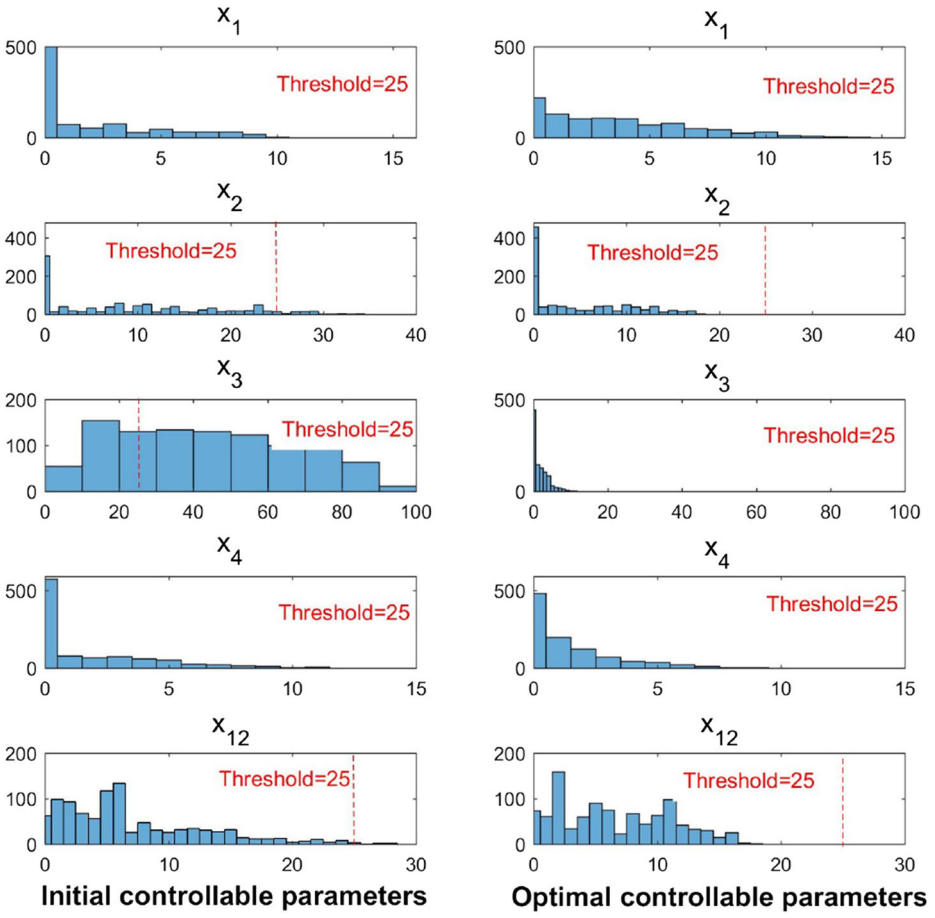

Fig. 11 Distribution of queue lengths when $L = 35$

Fleck et al. (2016). Three sets of simulations are presented below, one for each of the three cost metrics in Eqs. 14, 15 and 17.

6.1 Simulation results under the no traffic blocking assumption (A3)

In this section, we maintain Assumption (**A3**) and ignore any possible blocking effects.

1. Average Queue Cost Function We minimize metric (14), over $[0, T]$. All three arrival processes are Poisson with rates $\tilde{\alpha} = [0.41, 0.45, 0.32]$ and the departure rates at roads 1,2,3,4 are $[1.2, 1.3, 1.2, 1.1]$. We choose $T = 1000$s, $w_i = 1$ and $\theta_i \in [10, 50]$ for all i, and the initial θ_i values are $[40, 20, 20, 40]$. Figure 7 shows the optimal cost (averaged over 10 sample paths) considering the transit delay in the SFM between intersections (red curve) and ignoring this delay (blue curve) as a function of L. In this case, delay has no effect on the long term total average queue length, as expected. However, this metric may not accurately capture traffic congestion.

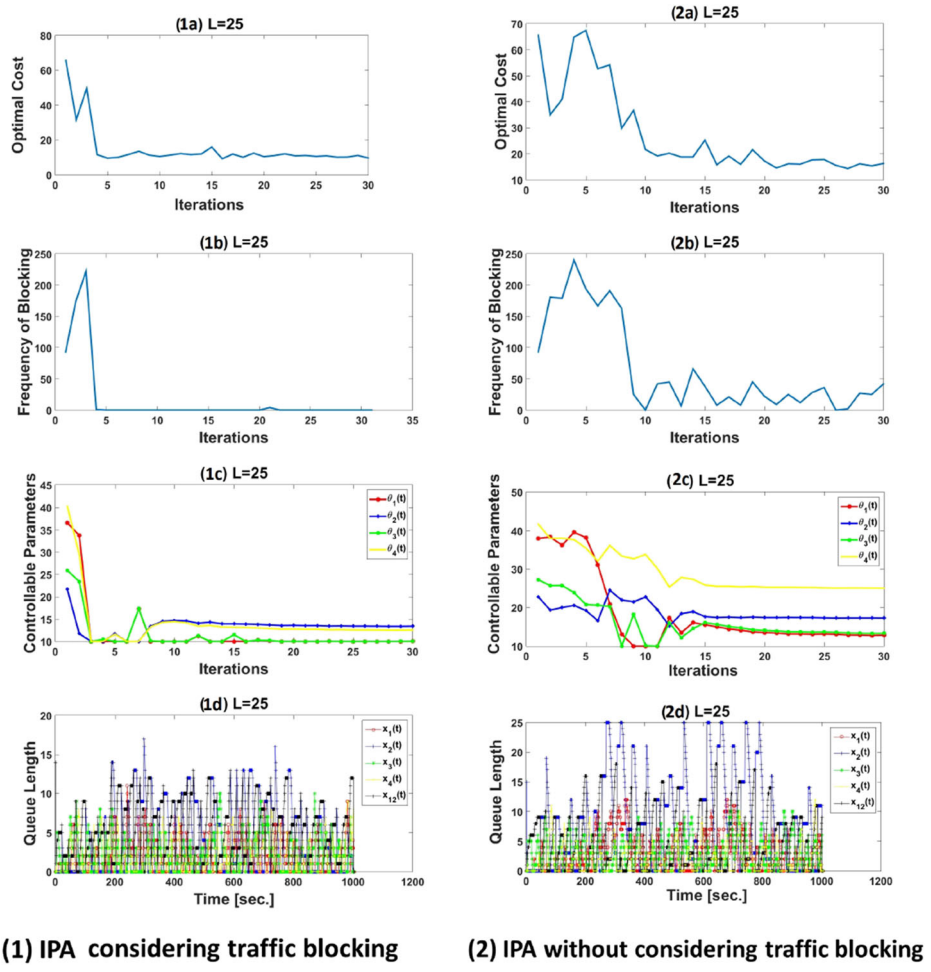

Fig. 12 Comparison of Average Cost when traffic blocking is ignored and when it is included when $L = 25$

2. Power Cost Function, $= 2$ For the same settings as before and a quadratic queuing cost, Fig. 8 shows how this cost function and the associated controllable parameters converge when $L = 100$, achieving a 40% cost decrease. In the left plot of Fig. 9, we use the SFM both including the transit delay and ignoring this delay in order to compare the optimal costs under these two models. Clearly, including delays in our IPA estimators for $L > 0$ achieves a lower cost, with the gap increasing as L increases.

3. Threshold Cost Function For the same settings and a common threshold $\zeta_i = 25$ for all i and with $L = 35$, Fig. 10 shows how this cost function and the associated controllable parameters converge, with the cost converging to its zero lower bound, therefore, in this case we see that our approach reaches the global optimum. In the right plot of Fig. 9, we apply the SFM considering both the transit delay between intersections and ignoring this delay so as to compare the resulting optimal costs. Once again, including delays achieves a lower cost, with the gap increasing as L increases.

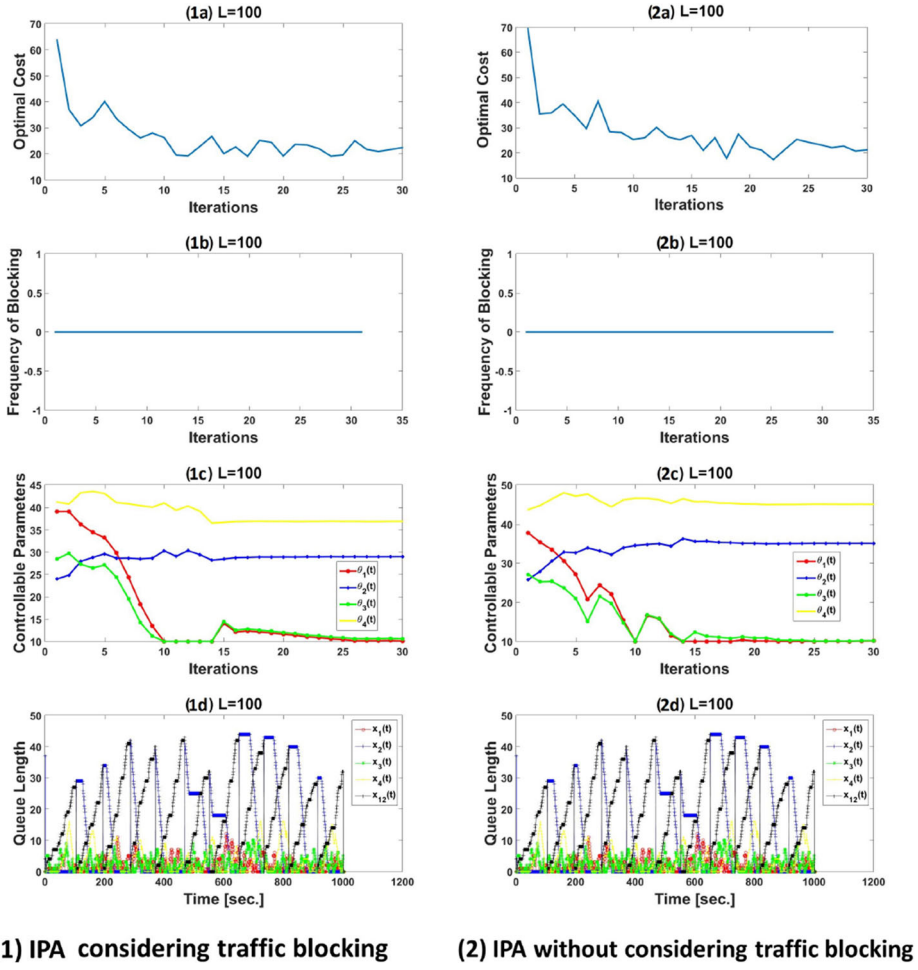

Fig. 13 Comparison of Average Cost when traffic blocking is ignored and when it is included when $L = 100$

In Fig. 11, we provide histograms of the queue contents when $L = 35$. On the left, the controllable parameters are at their initial values [40, 20, 20, 40] and we can see that queues 2, 3, and 12 frequently exceed the threshold. Under the optimal solution on the right, we observe that no queue ever exceeds the threshold over $[0, T]$, hence the optimal cost 0 is obtained. Moreover, note that the probabilities that $x_2(t) = 0$ and $x_3(t) = 0$ significantly increase indicating a much improved traffic balance.

6.2 Simulation results with traffic blocking included

In this section, we incorporate the effect of traffic blocking between intersections using the IPA derivative estimates derived in Section 5, so as to demonstrate improved traffic light assignments and result in performance improvements as well. As in the previous section, we consider in what follows each of the three cost functions we have defined.

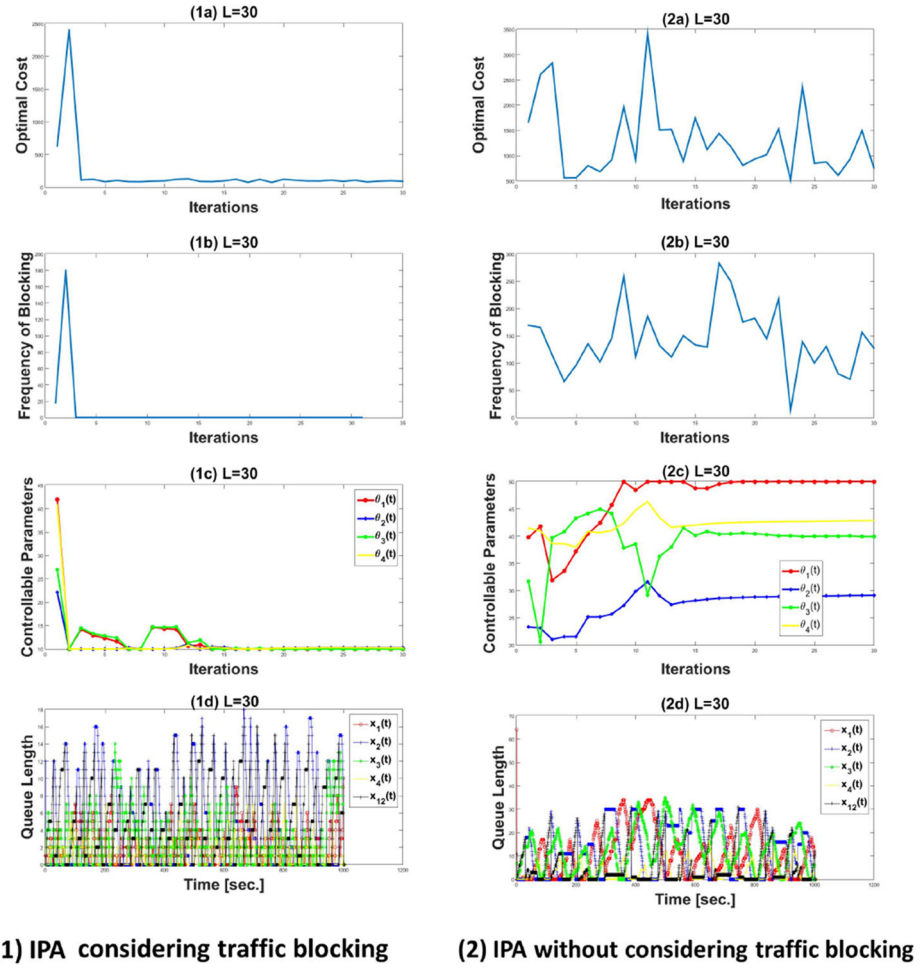

Fig. 14 Comparison of Power Cost when traffic blocking is ignored and when it is included when $L = 30$

1. Average Queue Cost Function All three arrival processes are Poisson with rates $\tilde{\alpha} = [0.43, 0.49, 0.34]$ and the departure rates at roads 1,2,3,4 are [1.2, 1.3, 1.2, 1.1]. We choose $T = 1000$s, $w_i = 1$ and $\theta_i \in [10, 50]$ for all i, and the initial θ_i values are $[43, 22, 24, 41]$. Figure 12 shows the comparison between the method with and without considering traffic blocking when $L = 25$. The left plots (1) provide results when IPA estimates consider traffic blocking while the right plots (2) are when IPA estimates are used without considering traffic blocking. The figures with sub-labels (a), (b) and (c) respectively show how the cost function, the blocking frequency, and the associated controllable parameters converge. The plots with sub-label (d) show the vehicle queue length in each road after convergence.

In this case, since the short length $L = 25$ allows for several instances of blocking as seen in the plot (2c), using the IPA estimates in Section 5 achieves a 33% cost decrease and eliminates all blocking. On the other hand, when $L = 100$, Fig. 13 shows that the IPA estimates considering and ignoring traffic blocking achieve almost the same cost since

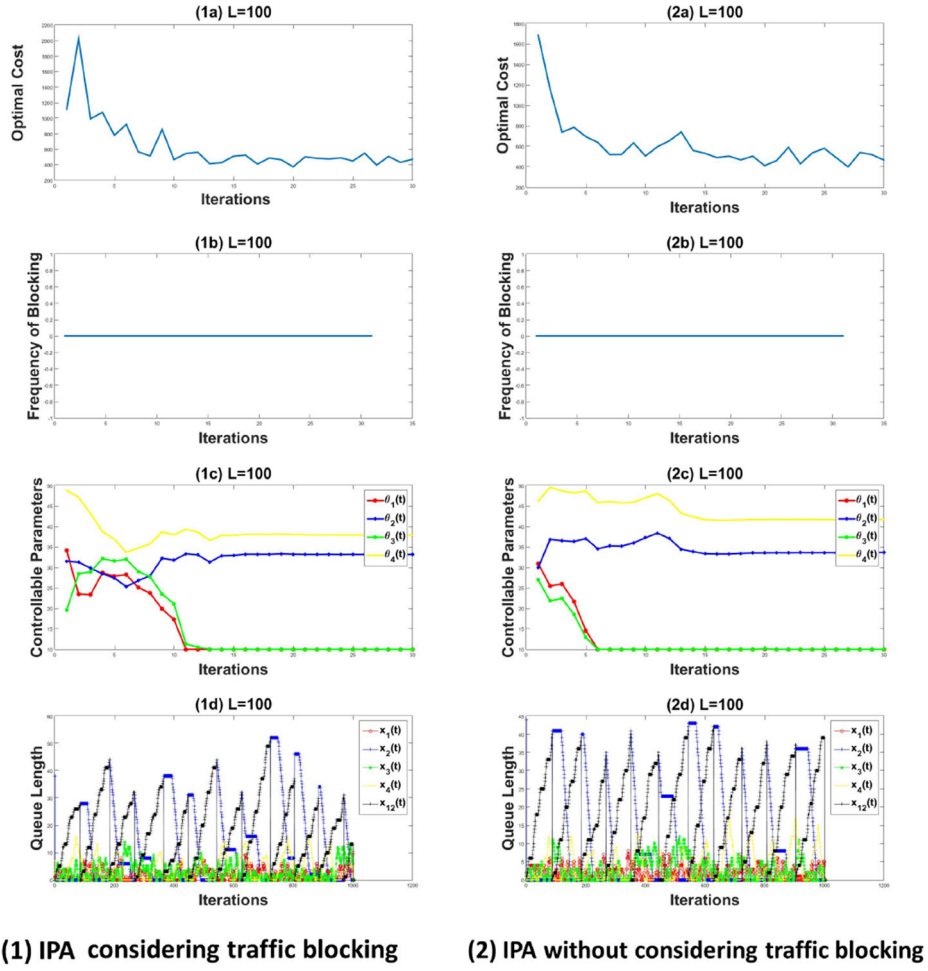

Fig. 15 Comparison of Power Cost when traffic blocking is ignored and when it is included when $L = 100$

the distance between intersections is large enough to ensure almost no occurrence of event $U2B$.

2. Power Cost Function, $= 2$. For the same settings as before, Fig. 14 compares the results obtained for IPA estimates with and without considering traffic blocking when $L = 30$. Using IPA estimates which account for blocking achieves a 75% cost decrease while again eliminating all blocking as shown in plots (1b) and (2b). When $L = 100$, Fig. 15 shows that IPA estimates considering and ignoring traffic blocking have the same performance because there is no occurrence of event $U2B$.

3. Threshold Cost Function All three arrival processes are Poisson with rates $\tilde{\alpha} = [0.53, 0.49, 0.34]$ and the departure rates at roads 1,2,3,4 are [1.2, 1.3, 1.2, 1.1]. We choose $T = 1000$s, $w_i = 1$ and $\theta_i \in [10, 50]$ for all i, and the initial θ_i values are [43, 22, 24, 41]. A common threshold $\zeta_i = 25$ is set for all i. Figure 16 shows that IPA estimates which include

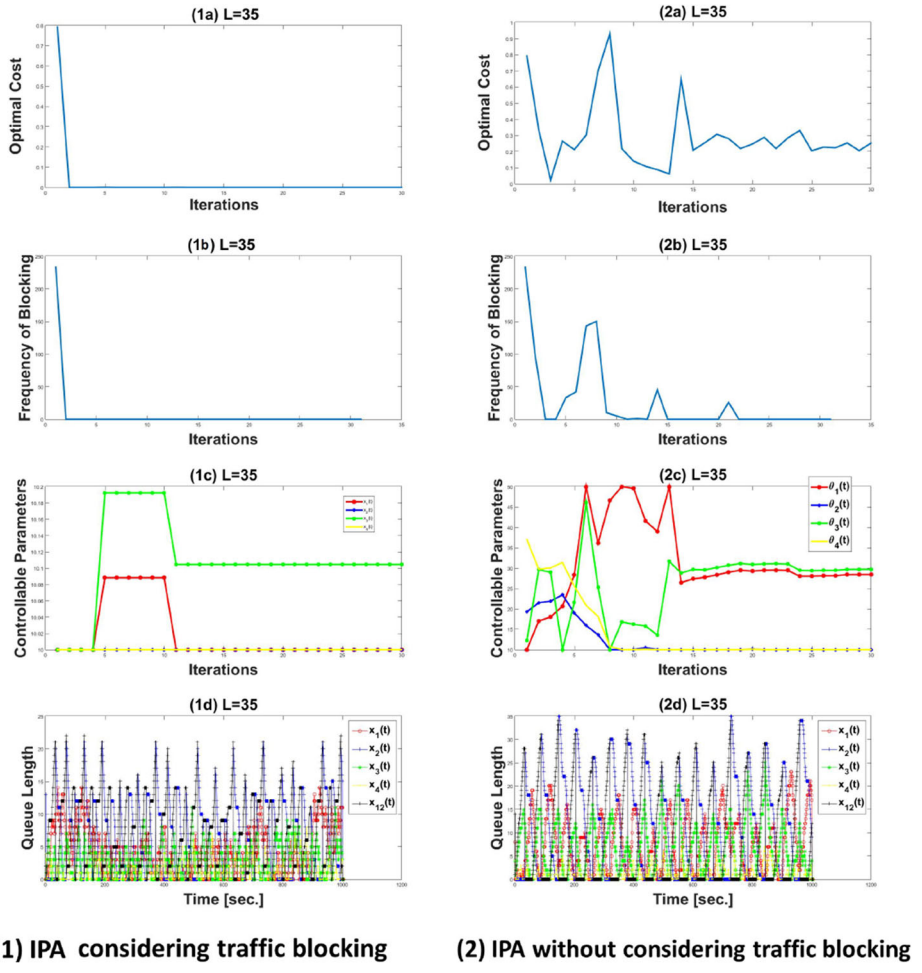

Fig. 16 Comparison of Threshold Cost when traffic blocking is ignored and when it is included when $L = 35$.

the effect of traffic blocking achieve a significant cost decrease relative to those ignoring traffic blocking. The frequency of blocking also converges to zero in the latter case, although the convergence rate is relatively low. This behavior is caused by the nature of the threshold cost function whose objective is to reduce the frequency that a queue length is larger than a threshold which is along the same lines as the objective to reduce the frequency of blocking.

7 Conclusions and future work

We have extended Stochastic Flow Models (SFMs) to allow for delays which can arise in the flow movement, as well as for possible blocking effects when the distance between nodes is relatively small. We have applied this framework to the multi-intersection traffic

light control problem by including transit delays for vehicles moving from one intersection to the next and derived the IPA derivative estimators for this extended SFM for three congestion cost metrics with respect to the controllable green/red cycle lengths, including two new cost metrics that better capture congestion. We have also derived IPA derivative estimators that include possible blocking effects due to the coupling between two nodes. Simulation results show that the inclusion of delays and blocking effects in our analysis leads to improved performance relative to models that ignore delays and/or blocking. Future work aims at demonstrating how this optimization framework scales up when the system considered includes a large number of nodes taking advantage of the event-driven nature of IPA whose complexity, therefore, scales with the number of events and not the (much larger) dimensionality of state space of a network.

Acknowledgments This work was supported in part by NSF under grants ECCS-1509084, DMS-1664644, and CNS-1645681, by AFOSR under grant FA9550-19-1-0158, by ARPA-E's NEXTCAR program under grant DE-AR0000796, and by the MathWorks.

References

Anderson MP, Woessner WW, Hunt RJ (2015) Applied groundwater modeling: simulation of flow and advective transport. Academic Press, Cambridge

Armony M, Israelit S, Mandelbaum A, Marmor YN, Tseytlin Y, Yom-Tov GB et al (2015) On patient flow in hospitals: a data-based queueing-science perspective. Stoch Syst 5(1):146–194

Cassandras CG, Wardi Y, Melamed B, Sun G, Panayiotou CG (2002) Perturbation analysis for on-line control and optimization of stochastic fluid models. IEEE Trans Autom Control 47(8):1234–1248

Cassandras CG, Lafortune S (2009) Introduction to discrete event systems. Springer, Berlin

Cassandras CG, Wardi Y, Panayiotou CG, Yao C (2010) Perturbation analysis and optimization of stochastic hybrid systems. Eur J Control 6(6):642–664

Chen R, Cassandras CG (2018) Stochastic flow models with delays and applications to multi-intersection traffic light control. Proc 2018 Intl Worksh Discret Event Syst 51(7):39–44

Fleck JL, Cassandras CG, Geng Y (2016) Adaptive quasi-dynamic traffic light control. IEEE Trans Control Syst Technol 24(3):830–842

Fu MC, Howell WC (2003) Application of perturbation analysis to traffic light signal timing. Proc IEEE, Conf on Decision and Control, pp 4837–4840

Geng Y, Cassandras CG (2012) Traffic light control using infinitesimal perturbation analysis. In: 2012 IEEE 51St annual conf. on decision and control (CDC). IEEE, pp 7001–7006

Geng Y, Cassandras CG (2015) Multi-intersection traffic light control with blocking. Discret Event Dyn Syst 25(1-2):7–30

Head L, Ciarallo F, Kaduwela DL (1996) A perturbation analysis approach to traffic signal optimization. INFORMS National Meeting

Panayiotou CG, Howell WC, Fu MC (2005) Online traffic light control through gradient estimation usinf stochastic flow models. Proc IFAC World Congress

Wardi Y, Adams R, Melamed B (2010) A unified approach to infinitesimal perturbation analysis in stochastic flow models: the single-stage case. IEEE Trans Autom Control 55(1):89–103

Yao C, Cassandras CG (2011) Perturbation analysis of stochastic hybrid systems and applications to resource contention games. Front Electr Electron Eng China 6(3):453–467

Yin S, Ding SX, Abandan Sari AH, Hao H (2013) Data-driven monitoring for stochastic systems and its application on batch process. Intl J Syst Sci 44(7):1366–1376

Rui Chen received the B.S. degree in School of Automation from Huazhong University of Science & Technology, Wuhan, China, in 2011, the M.S. degree from School of Electronic Information and Electrical Engineering, Shanghai Jiaotong University, Shanghai, China, in 2014. He is currently a Ph.D. candidate in systems engineering at Boston University, Boston, MA, USA. His research interests include traffic light control problems, the optimization of ride sharing systems and the optimal control of connected and autonomous vehicles.

Christos G. Cassandras (F'96) received the B.S. degree from Yale University, New Haven, CT, USA, in 1977, the M.S.E.E. degree from Stanford University, Stanford, CA, USA, in 1978, and the M.S. and Ph.D. degrees from Harvard University, Cambridge, MA, USA, in 1979 and 1982, respectively. He was with ITP Boston, Inc., Cambridge, from 1982 to 1984, where he was involved in the design of automated manufacturing systems. From 1984 to 1996, he was a faculty member with the Department of Electrical and Computer Engineering, University of Massachusetts Amherst, Amherst, MA, USA. He is currently a Distinguished Professor of Engineering with Boston University, Brookline, MA, USA, the Head of the Division of Systems Engineering, and a Professor of Electrical and Computer Engineering. He specializes in the areas of discrete event and hybrid systems, cooperative control, stochastic optimization, and computer simulation, with applications to computer and sensor networks, manufacturing systems, and transportation systems. He has authored over 400 refereed papers in these areas, and six books. Dr. Cassandras is a member of Phi Beta Kappa and Tau Beta Pi. He is also a Fellow of the International Federation of Automatic Control (IFAC). He was a recipient of several awards, including the 2011 IEEE Control Systems Technology Award, the 2006 Distinguished Member Award of the IEEE Control Systems Society, the 1999 Harold Chestnut Prize (IFAC Best Control Engineering Textbook), a 2011 prize and a 2014 prize for the IBM/IEEE Smarter Planet Challenge competition, the 2014 Engineering Distinguished Scholar Award at Boston University, several honorary professorships, a 1991 Lilly Fellowship, and a 2012 Kern Fellowship. He was the Editor-in-Chief of the IEEE TRANSACTIONS ON AUTOMATIC CONTROL from 1998 to 2009. He serves on several editorial boards and has been a Guest Editor for various journals. He was the President of the IEEE Control Systems Society in 2012.